

# Thermophysical Characterisation Methods and Uncertainty Considerations

## Content

- 1 Aim of Measurements and Standards
- 2 Applied Thermophysical Methods
- 3 Theory
- 4 Description of Methods
  - 4.1 Push Rod Dilatometry: DIL
  - 4.2 Dynamic Scanning Calorimetry: DSC
  - 4.3 Laser Flash Analysis: LFA
  - 4.4 Transient Hot Bridge: THB
  - 4.5 Heat Flow Meter: HFM
  - 4.6 Thermogravimetry with simultaneous DTA, FTIR, Mass Spectroscopy: STA
  - 4.7 Stabinger Viscometry SVM
- 5 Literature

Content	Table(s)	Figure(s)
<b>Measurements under the scope of accreditation *)</b>		
Linear Thermal Expansion: $\Delta L(T)/L_0$ ; $CTE(T)$	x-x-x	<input checked="" type="checkbox"/>
Specific Heat; Apparent Specific Heat: $c_p$ ; $c_p^{(app.)}$	x-x-x	<input checked="" type="checkbox"/>
Thermal Diffusivity: $a$	<input checked="" type="checkbox"/>	<input checked="" type="checkbox"/>
<b>Measurements out of the scope of accreditation *)</b>		
Density (from Geometry and Weight): $\rho$	x-x-x	<input checked="" type="checkbox"/>
Thermal Conductivity (calculated: $\lambda = a \times \rho \times c_p$ )	x-x-x	<input checked="" type="checkbox"/>
Density (Pycnometer, Archimedes): $\rho$	x-x-x	<input checked="" type="checkbox"/>
Viscosity and Density (Newtonian Fluids) : $\eta, \nu$	x-x-x	<input checked="" type="checkbox"/>
Thermal Conductivity (Transient Hot Bridge: THB): $\lambda$	x-x-x	<input checked="" type="checkbox"/>
Thermal Conductivity (Heat Flow Meter: HFM): $\lambda$	x-x-x	<input checked="" type="checkbox"/>
Specific Heat; Apparent Specific Heat: $c_p$ ; $c_p^{(app.)}$	x-x-x	<input checked="" type="checkbox"/>
Simultaneous Thermogravimetry – DTA; DSC; qMS; FTIR	x-x-x	<input checked="" type="checkbox"/>
Mass Spectroscopy	x-x-x	<input checked="" type="checkbox"/>
Fourier Transformed Infrared Spectroscopy	x-x-x	<input checked="" type="checkbox"/>
Thermo-kinetic Modelling	x-x-x	<input checked="" type="checkbox"/>
FE-simulation based on thermo-kinetic models	x-x-x	<input checked="" type="checkbox"/>

\*) .... Referes to: SKM\_C30819020410571 - 17025\_Akkreditierungsbescheid; SKM\_C30819020410560 - 17025\_Akkreditierungsbescheid; Beilage zum Bescheid GZ.: BMDW-92.221/0708-I/12/2018 Thermophysik\_17025T

# 1 Aim of Measurements and Standards

Thermophysical analysis: referred material(s) is (are) indicated on the cover sheet of the delivered report. The requested thermophysical data are specified by order.

**The adopt methods are applied in accordance to the requirements of the accreditation and/or in accordance to the standards as mentioned in Tab.1.**

**The uncertainties of measurement results are stated specific for each method. Typically, they scale less than 2% of the measured value. The uncertainties specific for each method are rechecked at the beginning of each measuring campaign. Uncertainties in measurement results higher than 2% of the measured value are to be drawn back to influences caused by the material or the specimen themselves.**

Method	Standard	Title (D)	Year
TA	DIN 51005	Thermische Analyse Begriffe	1999
GUM	DIN V ENV 13005	Leitfaden zur Bestimmung der Messunsicherheit beim Messen Guide to the expression of uncertainty in measurement	1999
DIL	DIN 51045 Teil 1	Bestimmung der thermischen Längenänderung fester Körper Grundlagen	1989
DIL	DIN 51045 Teil 2	Bestimmung der thermischen Längenänderung fester Körper unter Wärmeeinwirkung Prüfung gebrannter feinkeramischer Werkstoffe	1976
DIL	DIN 51045 Teil 3	Bestimmung der thermischen Längenänderung fester Körper unter Wärmeeinwirkung Prüfung ungebrannter feinkeramischer Werkstoffe	1976
DIL	DIN 51045 Teil 4	Bestimmung der thermischen Längenänderung fester Körper unter Wärmeeinwirkung Prüfung gebrannter grobkeramischer Werkstoffe	1976
DIL	DIN 51045 Teil 5	Bestimmung der thermischen Längenänderung fester Körper unter Wärmeeinwirkung Prüfung ungebrannter grobkeramischer Werkstoffe	1976
DIL	DIN EN 1159-1	Hochleistungskeramik - Keramische Verbundwerkstoffe, Thermophysikalische Eigenschaften Bestimmung der thermischen Ausdehnung	2009
DIL	DIN 51909	Bestimmung des linearen thermischen Ausdehnungskoeffizienten Feststoffe, Prüfung von Kohlenstoffmaterialien	1998
DIL	ISO 11359-2	Determination of coefficient of linear thermal expansion and glass transition temperature Plastics	1999
TG	DIN 51006	Thermogravimetrie Grundlagen	2000
DTA	DIN 51007	Differenzthermoanalyse Grundlagen	1994
DTA	DIN 51004	Bestimmung der Schmelztemperatur kristalliner Stoffe mit der Differenzthermoanalyse (DTA)	1994
DSC	DIN EN ISO 11357-4	Dynamische Differenz-Thermoanalyse (DSC) - Bestimmung der spezifischen Wärmekapazität Kunststoffe	2014
DSC	DIN V ENV 1159-3	Keramische Verbundwerkstoffe, thermophysikalische Eigenschaften Bestimmung der spezifischen Wärmekapazität	1995
DSC	ÖNORM EN 821-3	Hochleistungskeramik - Monolithische Keramik, Thermophysikalische Eigenschaften Bestimmung der spezifischen Wärme	2005
DSC	DIN V ENV 821 Teil 3	Hochleistungskeramik - Monolithische Keramik, Thermophysikalische Eigenschaften Bestimmung der spezifischen Wärme	1993
LF	DIN EN 821-2	Hochleistungskeramik - Monolithische Keramik, Thermophysikalische Eigenschaften Messung der Temperaturleitfähigkeit mit dem Laserflash- (oder Wärmepuls-) Verfahren	1997
LF	ÖNORM EN 1159-2	Hochleistungskeramik - Keramische Verbundwerkstoffe, Thermophysikalische Eigenschaften Bestimmung der Temperaturleitfähigkeit	2004
LF	DIN V ENV 1159 Teil 2	Hochleistungskeramik - Keramische Verbundwerkstoffe, Thermophysikalische Eigenschaften Bestimmung der Temperaturleitfähigkeit	1993
LF	DIN 51936	Prüfung von Kohlenstoffmaterialien Bestimmung der Temperaturleitfähigkeit bei hohen Temperaturen nach dem Laser Impuls Verfahren	2016
LF	ASTM E 1461-01	Standard Test Method for Thermal Diffusivity by the Flash Method Overview	2013
HFM	DIN EN 12667	Bestimmung des Wärmedurchlasswiderstandes nach dem Verfahren mit dem Plattengerät und dem Wärmestrommessplatten-Gerät Wärmetechnisches Verhalten von Baustoffen und Bauprodukten - Produkte mit hohem und mittlerem Wärmedurchlasswiderstand	2001
HFM	DIN EN 12664	Bestimmung des Wärmedurchlasswiderstandes nach dem Verfahren mit dem Plattengerät und dem Wärmestrommessplatten-Gerät Wärmetechnisches Verhalten von Baustoffen und Bauprodukten - Trockene und feuchte Produkte mit mittlerem und niedrigem	2001
HFM	DIN EN 12939	Bestimmung des Wärmedurchlasswiderstandes nach dem Verfahren mit dem Plattengerät und dem Wärmestrommessplatten-Gerät Wärmetechnisches Verhalten von Baustoffen und Bauprodukten - Dicke Produkte mit hohem und mittlerem	2000
HFM	ISO 8301	Determination of steady-state thermal resistance and related properties Thermal insulation, Heat flow meter apparatus	1991
HFM	ASTM C518	Standard Test Method for Steady-State Thermal Transmission Properties by Means of the Heat Flow Meter Apparatus	2017
HFM	JIS A1412	Test method for thermal resistance and related properties of thermal insulations. Part 1 Guarded hot plate apparatus	2016

Tab. 1: Methods and Standards

## 2 Applied Thermophysical Methods

### 2.1 Properties and Units:

Linear thermal expansion:  $\Delta L/L_0$ ;  $[\Delta L/L_0] = 1$

Coefficient of Linear Thermal Expansion:  $CTE \equiv \alpha$ ;  $[CTE] = 1/K$

Thermal density:  $\rho$ ;  $[\rho] = 1g/cm^3$

Specific heat:  $c_p$ ;  $[c_p] = 1J/g.K$

Thermal diffusivity:  $a$ ;  $[a] = 1m^2/s$

Thermal conductivity:  $\lambda$ ;  $[\lambda] = 1W/m.K$

Change of mass:  $\Delta m$ ;  $[\Delta m] = 1g$

Detection of mass:  $j$ ;  $[j] = 1A$ ; absorbance  $a_u$ ;  $[a_u] = 1$

Kinematic viscosity:  $\nu$ ;  $[\nu] = 1m^2/s$

Dynamic viscosity:  $\eta$ ;  $[\eta] = 1Pa.s$

### 2.2 Applied measuring methods to determine these material properties:

Push rod dilatometry (linear thermal expansion)

Dynamic scanning calorimetry - DSC (specific heat, Enthalpy, Phase transition)

Laser flash method (Thermal diffusivity)

$\lambda = \rho \times c_p \times a$ : Product of density, specific heat and thermal diffusivity

Thermal conductivity – calculated:

Heat Flow Meter HFM (thermal conductivity of solids; specific heat)

Transient Hot Bridge THB (thermal conductivity: solids, liquids, semi-solid formulations)

Microbalance with optional simultaneous DTA or DSC analysis, Fourier transformed Infrared Spectroscopy, Mass Spectroscopy

Stabinger Viscometry: (simultaneously: viscosity & density)

### 3 Theory

#### 3.1 Physics of the Measurement of Thermophysical Properties

The situation of spatial heat propagation in an inhomogeneous heated spatial area<sup>1</sup> is illustrated in Fig. 1. The material properties needed to describe the physical situation are the thermal conductivity  $\lambda$ , specific heat  $c_p$ , and the density  $\rho$ . One has to notice that these properties are dependent on the local composition of a material – thus on the vectorial position  $\vec{x}$  and from the local temperature at the time of observation  $T(\vec{x}, t)$ . The heat content  $Q_V(t)$  of a volume  $V$  is calculated with equation (3.1-1). In case of absence of any thermal source  $S_+$  or sink  $S_-$  any change of the heat content of this volume balances equal to 0 with the integral vectorial heat flux  $\vec{P}_{/A}(\vec{x}, t)$  through the surface of this volume. The local heat flux is determined by the local gradient of the temperature field  $\nabla T(\vec{x}, t)$  and the thermal conductivity of the conducting medium as described by Fourier's law (3.1-2). The balance equation is given in (3.1-3).

$$Q_V(t) = \int_V \rho(\vec{x}, T) \cdot \left[ \int_0^{T(\vec{x}, t)} c_p(\vec{x}, T) \cdot dT \right] \cdot dV \quad (3.1-1)$$

$$\vec{P}_{/A}(\vec{x}, t) = -\lambda(\vec{x}, T) \cdot \nabla T(\vec{x}, t) \quad (3.1-2)$$

$$\frac{dQ_V(t)}{dt} + \oint_{\partial V} d\vec{f} \cdot \vec{P}_{/A}(\vec{x}, t) = \left\{ \sum_i S_i^+ + \sum_j S_j^- \right\} \quad (3.1-3)$$

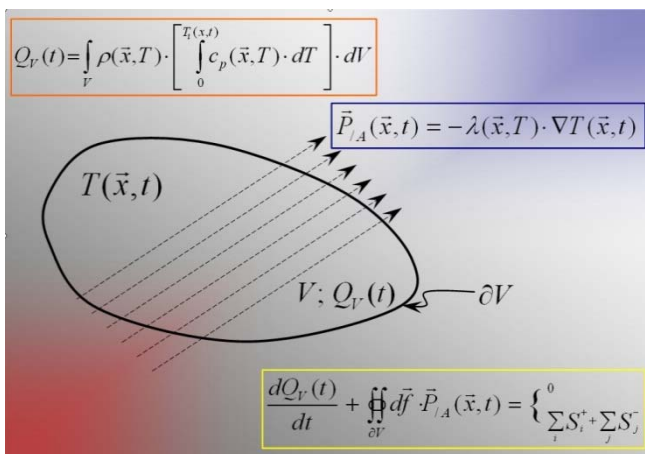


Fig. 1: Heat balance in a Volume<sup>2</sup>

Under the assumption of a conservative system, of homogeneity of the thermally conducting medium (no spatial dependence of the material properties thermal conductivity  $\lambda$ , specific heat  $c_p$ , and the density  $\rho$ ) and of the neglect of any non-linearity, the balance equation (3.1-3) leads to Fourier's thermal conductivity equation (3.1-4). This equation defines the interrelationship between the four thermophysical basic properties:  $\lambda(T)$ ,  $c_p(T)$ ,  $\rho(T)$  and the thermal diffusivity  $a(T)$ . In general the thermal diffusivity  $a(T)$  defines the so called transport coefficient of the thermal conductivity problem. It's meaning is conform to the interpretation of the diffusivity coefficient of a diffusion problem. The specification to a transient but one dimensional phenomenon leads to the solution  $T(x, t)$  given in equation (3.1-5).  $U$ ,  $V$  and  $c$  are constants. With respect to the structure of the differential equation they become specified by two boundary conditions and one initial condition.

$$\frac{\partial T(\bar{x}, t)}{\partial t} = \left[ \frac{\lambda(T)}{\rho(T) \cdot c_p(T)} \right] \cdot \Delta T(\bar{x}, t) := a(T) \cdot \Delta T(\bar{x}, t) \quad (3.1-4)$$

$$T(x, t) = e^{-ct} \cdot \left[ U \cdot \sin \sqrt{\frac{c}{a}} \cdot x + V \cdot \cos \sqrt{\frac{c}{a}} \cdot x \right] \quad (3.1-5)$$

## 3.2 Uncertainty of Measurement Results

### 3.2.1 Principles to the GUM / ENV 13005 – Guide to Express Uncertainty of Measurement Results

As it is formulated in ENV 13005 the statement of the result of a measurement only is complete if it contains both, the value attributed to the measurand, and the uncertainty of measurement associated with this value<sup>3,4</sup>. In general, the theoretical formulation of a physical quantity  $Y$  is a function of  $N$  different input variables  $X_i$  (3.2-1). Each input variable  $X_i$  has to be measured repeatedly. The best estimate of an input quantity  $X_i$  is the arithmetic mean  $q_i$  of a number of  $n$  individual measurements  $\{q_{i,1}, q_{i,2}, \dots, q_{i,k}, \dots, q_{i,n}\}$  (3.2-2). The best estimate of the uncertainty of an individual  $q_{i,k}$  is the standard deviation of the individual measurements  $s(q_{i,k})$  (3.2-3). The uncertainty of the arithmetic mean of the full set of  $\{q_{i,k}\}$  is  $u(q_i)$ . It is given in equation (3.2-4). The best output estimate  $y$  is calculated from equation (3.2-5), using the best input estimates  $q_i$  for the input variables  $X_i$  as shown in equation (3.2-2). Finally the uncertainty of the output estimate  $u_c(y)$  is calculated by equation (3.2-6). It is called “*standard uncertainty of the output estimate*”.

$$Y = f(X_1, X_2, \dots, X_i, \dots, X_n) \quad (3.2-1)$$

$$q_i = \frac{1}{n} \cdot \sum_{k=1}^n q_{i,k} \quad (3.2-2)$$

$$s(q_{i,k}) = \sqrt{\frac{1}{n-1} \cdot \sum_{k=1}^n (q_{i,k} - q_i)^2} \quad (3.2-3)$$

$$u(q_i) = \frac{1}{\sqrt{n}} \cdot s(q_{i,k}) := u(x_i) \quad (3.2-4)$$

$$y = f(q_1, q_2, \dots, q_i, \dots, q_N) \quad (3.2-5)$$

$$u_c^2(y) = \sum_{i=1}^N \left( \frac{\partial f}{\partial x_i} \right)^2 \cdot u^2(x_i) \quad (3.2-6)$$

Equation (3.2-6) is well known as the Gaussian Error Propagation Law. It is to be noticed, that in correct measurements no errors are done: they will be eliminated at their earliest indication of evidence. Thus in terms of uncertainty considerations it's interpretation as a “*quadratic addition theorem of linear independent components of uncertainty*” should preferably be used.

Equation (3.2-6) calculates the standard uncertainty of the output estimate with respect to a 66% confidence interval. Usually measurement results of technical data are attributed with uncertainties of a 95% confidence interval. Thus results from equation (3.2-6) have to be multiplied with a coverage factor  $k = 2$  (3.2-7).

$$u_{c;95\%}^2(y) = 2 \cdot \sum_{i=1}^N \left( \frac{\partial f}{\partial x_i} \right)^2 \cdot u^2(x_i) \quad (3.2-7)$$

### 3.2.2 Application of the GUM to Attribute Dues to the Uncertainty from their Causation

Dues to the uncertainty of the result of any measurement typically derive from the measurement device, the examining model and the measured samples themselves. Thus an *Equipment Specific Uncertainty ESU*, a *Model Specific Uncertainty MSU*, and a *Sample Related Uncertainty SSU* are considered as contributors to the combined standard uncertainty of the measurement result. Generalizing equation (3.2-2), zero quantities are added to the mean of input estimates (3.2-8). This still consequences the arithmetic mean to be the best estimate of the measurement result. But from postulate, the uncertainties of these zero quantities are attributed to equipment related effects – *ESU*, to model related effects – *MSU*, and to sample related effects – *SSU*: c.f. equation (3.2-9).

$$q = \frac{1}{m} \cdot \sum_{k=1}^m q_k + \sum C_j \quad C_j = 0 \forall j; u(C_j) \neq 0 \quad (3.2-8)$$

$$u_c^2(y) = \sum_{i=1}^N \left( \frac{\partial f}{\partial x_i} \right)^2 \cdot u^2(x_i) + \sum u^2(C_j) \quad (3.2-9)$$

## 4 Description of Methods

### 4.1 Push Rod Dilatometry

#### 4.1.1 Measuring Devices

The method<sup>5</sup> is used in accordance to the standards listed in Tab.1. There are two dilatometers NETZSCH DIL 402C in service. Each one is used in a specific temperature range:

- Low temperature dilatometer: range of application [-180°C, +500°C]
- High temperature dilatometer: range of application [ $T_R$ , +1600°C]



Fig. 2: Push rod dilatometer with sample carrier, push rod and sample (red)

Both dilatometers are used under Helium or Argon conditions. Details of service conditions are documented in the data sheets of any order (appendix). As a matter of principle service is programmed in 12 or 24 hours intervals. Heating rates typically range about 2 K/min. This is in accordance with the relevant standards (Tab. 1) and leads to sufficiently low uncertainties. Based on measurements with reference materials<sup>1</sup> the uncertainty is less than 1% of the measured value.

#### 4.1.2 Principle of Measurement

The measuring process is done in two steps starting with the determination of the expansion behaviour of the dilatometer itself (correction function  $K$ ) and the measurement of specimen afterwards. From statistical reasons both types of measurements are carried out several times.

The value of the thermal expansion typically refers to reference-temperature  $T_0 = 20^\circ\text{C}$ . The subscriptions  $R$ ,  $Lit$  and  $S$  indicate measurements done with a reference material  $R$ , or a specimen  $S$ , or refer to reference data from literature  $Lit$  respectively. The physical definition of the linear thermal expansion  $\Delta L_R(T)/L_{0;R}$  and the knowledge of the thermal expansion behaviour of a reference material  $P_R(T)/L_{0;R}$  enable to derive the equation for the correction function  $K_R(T)$  (4.1-1). Using equation (4.1-2),  $K_R(T)$  enables calculation of linear

<sup>1</sup> Typically: Sapphire, Fused Silica, Alumina or Platinum

thermal expansion data of an unknown material (sample:  $S$ ) from subsequent measurements of the temperature dependent position  $P_S(T)$ .

$$K_R(T) = \left( \frac{\Delta L_R(T)}{L_{0,R}} \Big|_{Lit} - \frac{P_R(T)}{L_{0,R}} \right) \quad (4.1-1)$$

$$\frac{\Delta L_S(T)}{L_{0,S}} = \frac{P_S(T)}{L_{0,S}} + K_R(T) = \frac{P_S(T)}{L_{0,S}} + \left( \frac{\Delta L_R(T)}{L_{0,R}} \Big|_{Lit} - \frac{P_R(T)}{L_{0,R}} \right)$$

$$CTE_S(T) \equiv \alpha_S(T) := \frac{1}{\Delta T(T)} \cdot \frac{\Delta L_S(T)}{L_{0,S}} \quad (4.1-2)$$

Per definition, the thermal expansion  $\Delta L(T)/L_0$  and the coefficient of linear thermal expansion  $CTE(T) \equiv \alpha(T)$  refer to an initial temperature: preferably  $T_0 = 20^\circ\text{C}$ . Under real labor conditions measurements start at room temperatures  $T_R \neq 20^\circ\text{C}$ . Thus, a coordinate transformation is applied, fulfilling the condition:  $\Delta L(T=20^\circ\text{C}) := 0$ . The procedure is illustrated in Fig. 3. From equations (4.1-3) the correction of the thermal expansion data at the starting temperature  $T_S$  of the measurement and the corrected numbers of  $\Delta L(T)/L_0$  are calculated.

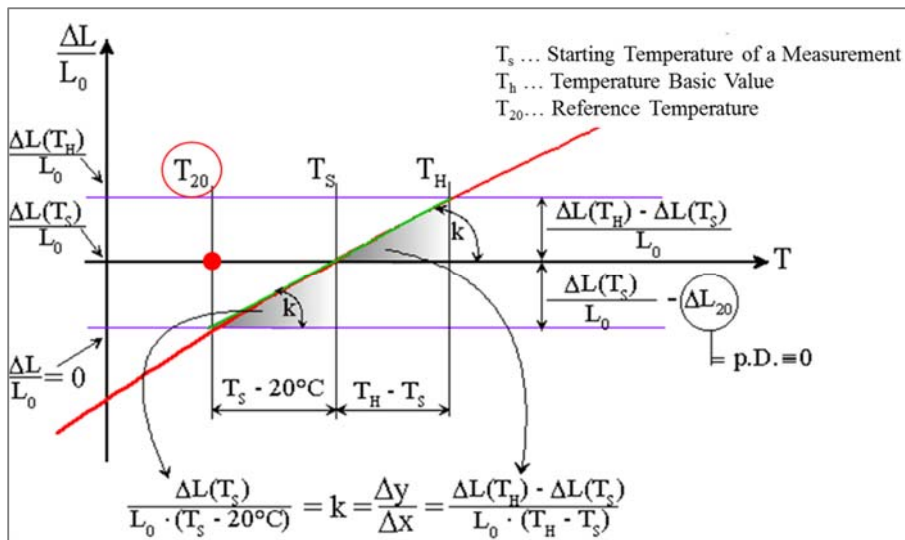


Fig. 3: Coordinate transformation of the curve of thermal expansion.

$$\frac{\Delta L(T_s)}{L_0} = \frac{\Delta L(T_h) - \Delta L(T_s)}{L_0(T_h - T_s)} \cdot (T_s - 20^\circ\text{C}) \quad (4.1-3)$$

$$\frac{\Delta L(T)}{L_0} = \frac{\Delta L(T)}{L_0} \Big|_{gemessen} + \frac{\Delta L(T_s)}{L_0} \Big|_{Korr}$$

The expansion behavior of pasts, highly viscose liquids and melts is measured in containers<sup>6</sup>. After melting the linear description switches over to the volumetric description. In axial orientation a *CTE*-value  $\alpha_s'$  is detected. In the liquid state it  $\alpha_s'$  is a superposition of both, the expansion behaviour of the liquid and the thermal expansion of the solid container. In radial direction only  $\alpha_c$  happens. This is the thermal expansion of the solid container. The linear thermal expansion of the liquid can be calculated by equation (4.1-4).

$$\frac{\Delta L_S}{L_{0;S}} = \sqrt[3]{(1 + \alpha_s' \cdot \Delta T) \cdot (1 + \alpha_c \cdot \Delta T)^2} - 1 \quad (4.1-4)$$

### 4.1.3 Uncertainty Concept:

To calculate uncertainties of  $\Delta L_S(T)/L_{0;S}$  and  $CTE_S(T)$  (3.2-7) is applied to (4.1-1) and (4.1-2). The concept is summarized in Fig. 4. The *ESU* is estimated from the non-linearity of the LVDT (Linear Variable Differential Transformer) of the device. It is monitored regularly but minimum once a year during the regular annual inspection. It scales in a range of 0,01% of the measured change of length – and can therefore not be represented in the figures in many cases. Contributions to the *MSU* result from the uncertainty of reported expansion data of the reference material used to perform the correction function  $K(T)$  – typically 1%, maximum 3% – and from the measurements needed therefore. Thus it scales with the value of the thermal expansion too. Contributions to the *SSU* result from the behaviour of the samples during the measurements. *SSU* varies randomly therefore – and possibly in a wide range.

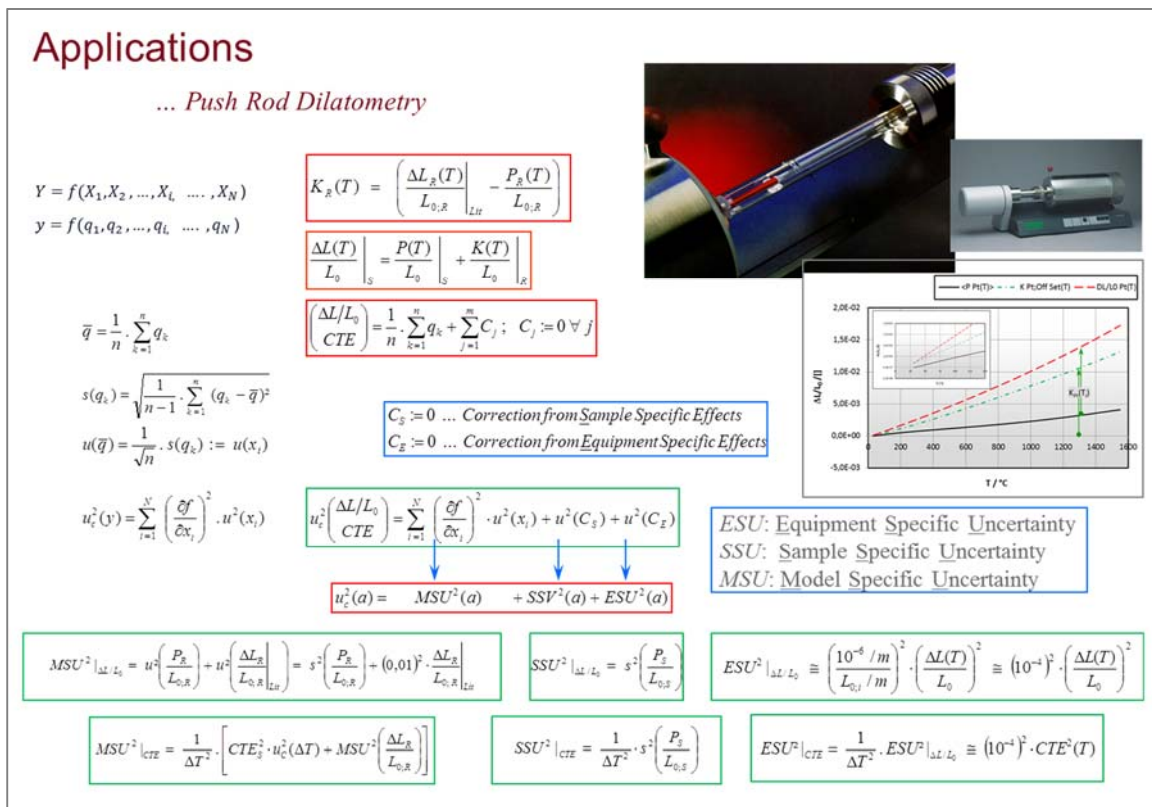


Fig. 4: Concept to formulate uncertainty contributions in push rod dilatometry

From mathematical reasons, the combined standard uncertainty of the linear coefficient of thermal expansion  $u_c(CTE_S(T))$  shows a singularity at the reference-temperature  $T_0$  (c.f. Fig. 3). Because of unavoidable uncertainties of both, the temperature detection of the device and the expansion detection, at temperatures near to  $T_0$  the uncertainties of  $\Delta L$  and  $\Delta T$  scale in the same range than  $\Delta L$  und  $\Delta T$  themselves. This causes senseless  $CTE$  results and the coefficient of linear thermal expansion  $CTE_S(T)$  features huge uncertainties near to  $T_0$ . So far the expansion behaviour near  $T_0$  shows a negligible curvature, a polynomial approximation can be used to smoothen the  $CTE(T)$  curve within a temperature interval  $[T_L, T_R]$ . This is illustrated in Fig. 5. A polynomial  $P_3(T)$  ensures a mathematically smooth transition. To establish an uncertainty model inner  $[T_L, T_R]$  a linear approximation of the polynomial  $P_3(T)$  can be used. It can be shown, that the uncertainty of the polynomial approximation is sufficiently estimated by equation (4.1-5)<sup>7</sup>.

$$u_c^2(P_{CTE}(T)) \leq 2 \cdot u^2(CTE(T_L)) \quad (4.1-5)$$

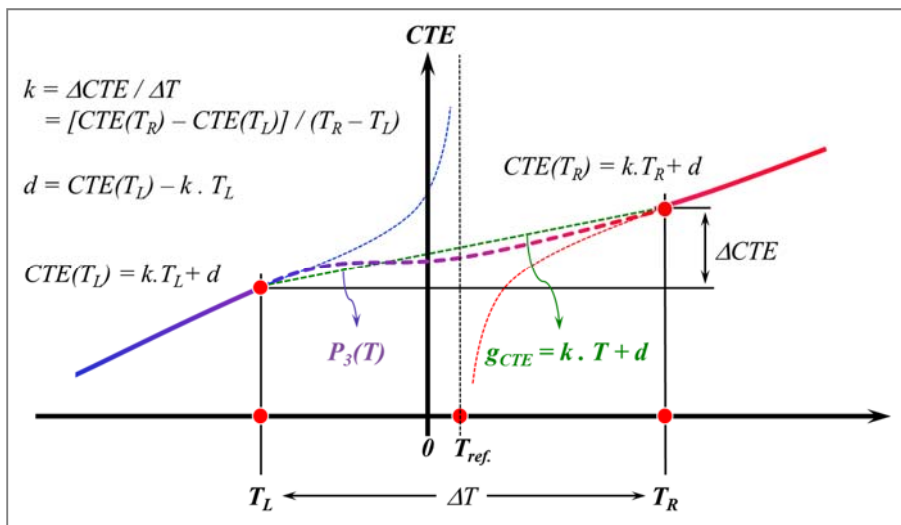


Fig. 5: Polynomial approximation to smoothen the  $CTE(T)$  curve within a temperature interval  $[T_L, T_R]$ .

#### 4.1.4 Results of Dilatometric Measurements:

For example in a temperature range  $[-180^\circ\text{C}, 1600^\circ\text{C}]$  the thermal expansion of an alumina material is shown in Fig. 6. Thermo-physics typically defines  $T_{Ref.}$  is  $20^\circ\text{C}$  as reference temperature. In a temperature range  $[-180^\circ\text{C}, 20^\circ\text{C}]$  data from the Low-Temperature-Dilatometer are used. This results in two different characteristics for the  $MSU|_{\Delta L/L_0}$  and  $SSU|_{CTE}$  as well.  $MSU|_{\Delta L/L_0}$  is about 1% of the measured thermal expansion.  $MSU|_{CTE}$  converges to less than 2% of the measured  $CTE$  value. From mathematical reasons  $MU|_{CTE}$  shows a singularity at  $T_{Ref.}$ . The smooth characteristics of  $\Delta L/L_0$  at  $T_{Ref.}$  allows a polynomial approximation of the  $CTE$  curve within  $[-80^\circ\text{C}, 150^\circ\text{C}]$ . On the basis of this approximation no singularity of the standard uncertainty  $u_c(CTE)$  occurs. The combined standard uncertainty of thermal expansion data of a thermally inert material like  $\text{Al}_2\text{O}_3$  can be estimated with less than 1% of the measured value. The combined standard uncertainty of the linear coefficient of thermal expansion of a thermally inert material ( $\text{Al}_2\text{O}_3$ ) converges to approximately 1% of the measured value. Near reference temperature uncertainty scales with less than 5% of the measured value so far a modelling of the  $CTE$  within a sufficiently wide interval  $[T_R; T_L]$  is done.

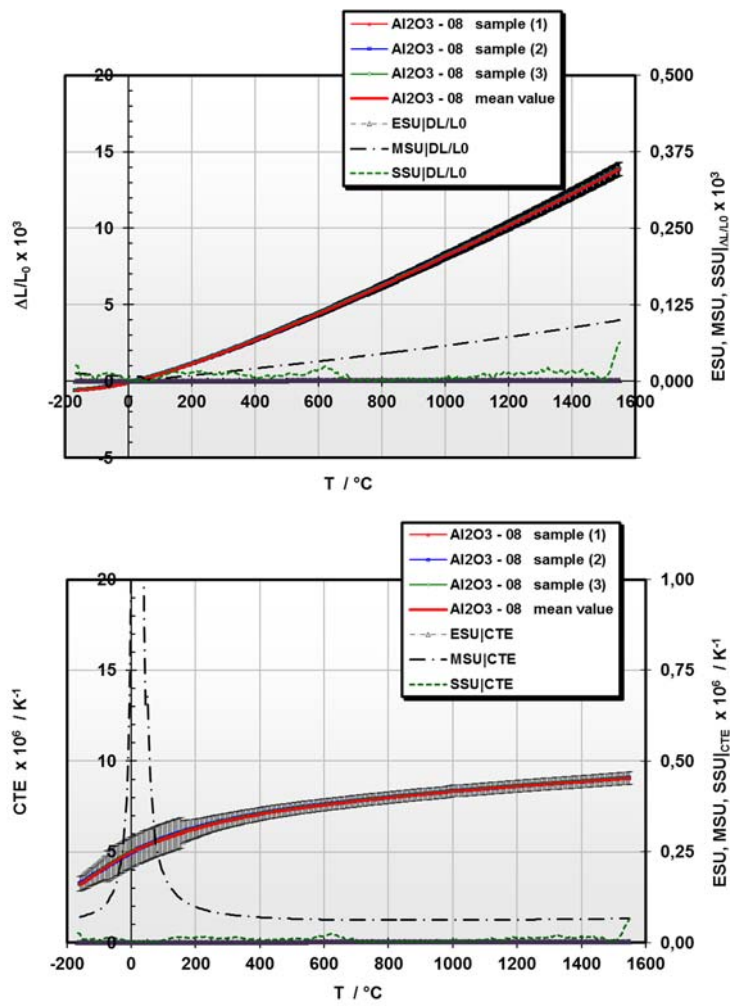


Fig. 6: Thermal expansion and linear coefficient of thermal expansion of  $Al_2O_3$

## 4.2 Dynamic Scanning Calorimetry DSC

### 4.2.1 Measuring Devices

The method<sup>8</sup> is used in accordance to the standards listed in Tab.1. Two calorimeters NETZSCH DSC 404C and a NETZSCH DSC 204 F1 Phoenix with an automatized sample changer are in service. Each one is used in a specific temperature range:

- Low temperature calorimeter (NETZSCH DSC 404C and a NETZSCH DSC 204 F1):  
range of application [-160°C, +600°C]
- High temperature calorimeter (NETZSCH DSC 404C):  
range of application [ $T_R$ , +1600°C]



Fig. 7: left: DSC 404C with sample carrier and sensor  
right: DSC 204 F1 Phoenix with an automatized sample changer

### 4.2.2 Principle of Measurement

As a matter of principle both calorimeters operate dynamically under Helium or Argon conditions. Heating rates typically scale between 10 K/min and 20 K/min. This is in accordance with the relevant standards (Tab. 1) and leads to sufficiently low uncertainties. Details of service conditions are documented in the data sheets of the report (appendix). Based on measurements with reference materials<sup>2</sup> the uncertainty is some 1% of the measured value.

The measuring process is done in three steps starting with the determination of the behaviour of the empty calorimeter (base line:  $B$ ), the measurement of a reference (e.g. sapphire measurement:  $R$ ), and the measurement of sample (sample measurement:  $S$ ). From statistical reasons all types of measurements are carried out several times.

The physical definition of the specific heat  $c_p(T)$  in equation (4.2-1) and the mathematical description of the heat content of a material as a function of temperature (equation (4.2-2)) enables to derive the dynamic calorimeter equation (4.2-5). Based on the measured DSC data from this equation the specific heat can be calculated. In equation (4.2-2)  $V$  means the volume of the sample and  $\rho$  the density. In equation (4.2-5)  $DSC$  means the sensor signal. The subscriptions  $B$ ,  $R$  and  $S$  indicate the type of the measurement as mentioned above.

---

<sup>2</sup> Typically Sapphire

$$\Delta Q = c_p \cdot m \cdot \Delta T \leftrightarrow c_p = \frac{\Delta Q}{m \cdot \Delta T} = \frac{Q|_T^{T+dT}}{m \cdot dT}; \quad [c_p] = 1 \frac{J}{g \cdot K} \quad (4.2-1)$$

$$Q(t) = \int_V dV \cdot \rho(\bar{x}, T) \cdot \int_0^{T_i(\bar{x}, t)} c_p(\bar{x}, T) \cdot dT \quad (4.2-2)$$

Equation (4.2-1) leads to (4.2-3). In the dynamic calorimeter the heat necessary to change the temperature of a sample is represented by the *DSC* signal. One obtains  $DSC^{(R)}$  when a reference material is measured,  $DSC^{(B)}$  for the measurement of a base line and  $DSC^{(S)}$  for the measurement of an unknown sample. To ensure an optimum representation of the occurring heat consumptions baseline corrected DSC signals are used (4.2-4)

$$dT(T) = \frac{Q^{(R)}|_T^{T+dT}}{m_R \cdot c_p^R(T)} = \frac{Q^{(S)}|_T^{T+dT}}{m_S \cdot c_p^S(T)} \quad (4.2-3)$$

$$\begin{aligned} Q^{(R)}|_T^{T+dT} &= DSC^{(R)}(T) - DSC^{(B)}(T) \\ Q^{(S)}|_T^{T+dT} &= DSC^{(S)}(T) - DSC^{(B)}(T) \end{aligned} \quad (4.2-4)$$

From (4.2-3) an expression for  $c_p^{(S)}(T)$  as given in (4.2-5).

$$c_p^{(S)}(T) = \frac{DSC^{(S)}(T) - DSC^{(B)}(T)}{DSC^{(R)}(T) - DSC^{(B)}(T)} \cdot \frac{m^{(R)}}{m^{(S)}} \cdot c_p^{(R)}(T) \quad (4.2-5)$$

To derive the combined standard uncertainty of the measurement results of the specific heat equation (4.2-5)<sup>9</sup> is used. The functions  $DSC(T)$  and  $f_E(T)$  are defined in equations (4.2-6). These functions are used in the overviewing Fig. 8.

$$\begin{aligned} f_E(T) &= \frac{m^{(R)}}{m^{(S)}} \cdot c_p^{(R)}(T) \\ DSC(T) &= \frac{DSC^{(S)}(T) - DSC^{(B)}(T)}{DSC^{(R)}(T) - DSC^{(B)}(T)} \end{aligned} \quad (4.2-6)$$

### 4.2.3 Uncertainty Concept:

To calculate uncertainty of  $c_p(T)$  (3.2-7) is applied to equations (4.2-5). Fig. 8 overviews the concept. The *ESU* is estimated from the deviations of the baselines of the device. It is monitored regularly and minimum measured three times at the beginning of any measuring campaign. Standard deviations of the base lines scale in a range of 1% of the measured value. Contributions to the *MSU* result from the uncertainty of reported  $c_p(T)$  data of the reference material used (typically sapphire). Once more standard deviations of the measured sapphire data scale in a range of 1% of the measured values. Contributions to the *SSU* result from the behaviour of the samples during the measurements. *SSU* varies randomly therefore – and possibly in a wide range.

# Applications

... Dynamic Scanning Calorimetry

$$Y = f(X_1, X_2, \dots, X_L, \dots, X_N)$$

$$y = f(q_1, q_2, \dots, q_L, \dots, q_N)$$

$$c_p^{(S)}(T) = \left[ \frac{DSC^{(S)}(T) - DSC^{(R)}(T)}{DSC^{(R)}(T) - DSC^{(B)}(T)} \right] \cdot \left[ \frac{m^{(R)}}{m^{(S)}} \cdot c_p^{(R)}(T) \right] =: [DSC(T)] \cdot [f_{\tilde{z}}(T)]$$

$$\bar{q} = \frac{1}{n} \cdot \sum_{k=1}^n q_k$$

$$s(q_k) = \sqrt{\frac{1}{n-1} \cdot \sum_{k=1}^n (q_k - \bar{q})^2}$$

$$u(\bar{q}) = \frac{1}{\sqrt{n}} \cdot s(q_k) := u(x_i)$$

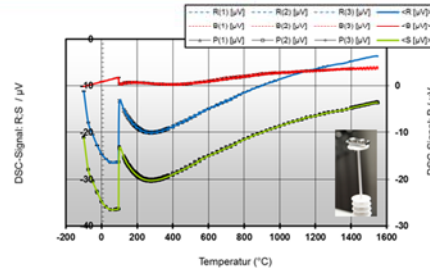
$$u_c^2(y) = \sum_{i=1}^N \left( \frac{\partial f}{\partial x_i} \right)^2 \cdot u^2(x_i)$$

$$c_p = \frac{1}{n} \cdot \sum_{k=1}^n c_{p,k} + \sum_{j=1}^m C_j; C_j := 0 \forall j$$

NO Correction needed  
XZ / 2013 (1)

$$u_c^2(c_p) = \sum_{i=1}^N \left( \frac{\partial f}{\partial x_i} \right)^2 \cdot u^2(x_i)$$

$$u_c^2(a) = ESU^2(a) + MSU^2(a) + SSU^2(a)$$



ESU: Equipment Specific Uncertainty  
SSU: Sample Specific Uncertainty  
MSU: Model Specific Uncertainty

$$ESU^2|_{c_p} \equiv f_{\tilde{z}}^2 \cdot \frac{(DSC^{(S)} - DSC^{(R)})^2}{(DSC^{(R)} - DSC^{(B)})^2} \cdot u^2(DSC^{(B)})$$

$$SSU^2|_{c_p} \equiv f_{\tilde{z}}^2 \cdot \frac{u^2(DSC^{(S)})}{(DSC^{(R)} - DSC^{(B)})^2}$$

$$MSU^2|_{c_p} \equiv f_{\tilde{z}}^2 \cdot \frac{(DSC^{(S)} - DSC^{(B)})^2}{(DSC^{(R)} - DSC^{(B)})^2} \cdot u^2(DSC^{(R)}) + DSC^2(T) \cdot \left( \frac{m^{(R)}}{m^{(S)}} \right)^2 \cdot u^2(c_p^{(R)})$$

Fig. 8: Concept to formulate uncertainty contributions in dynamic scanning calorimetry DSC

## 4.2.4 Results of DSC Measurements:

For example in a temperature range [-120°C, 1600°C] specific heat of sapphire is shown in Fig. 9. In a temperature range [-120°C, ~200°C] data from the Low-Temperature-Calorimeter are used. Because of the different types of sensors this results in different characteristics for the  $ESU|_{c_p}$ ,  $MSU|_{c_p}$  and  $SSU|_{c_p}$ . Nevertheless the curves for  $c_p$  and  $ESU|_{c_p}$  merge smoothly. Values for the  $MSU|_{c_p}$  scale significantly less than 0,5% of the measured specific heat. Values for the  $ESU|_{c_p}$  can be neglected. The combined standard uncertainty of a thermally inert material like sapphire can be estimates with approximately 0,5% of the measured value.

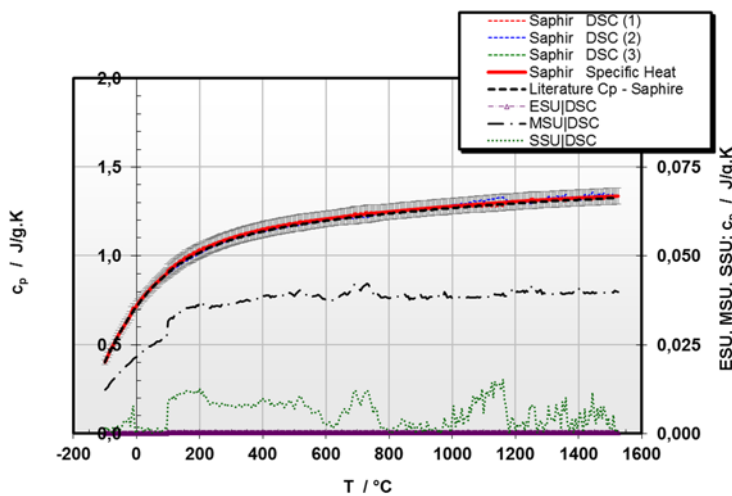


Fig. 9: Specific heat of sapphire

## 4.3 Laser Flash Method

### 4.3.1 Measuring Devices

The method<sup>10</sup> is used in accordance to the standards listed in Tab.1. Two equipment are in service.

- NETZSCH LFA 427: it can be equipped with two furnaces – applicable in two temperature ranges
  - Low temperature range of application [-120°C, +450°C]
  - High temperature range of application [ $T_R$ , +1600°C]
- NETZSCH LFA 467 Hyper Flash:
  - Temperature range of application [-100°C, +500°C]

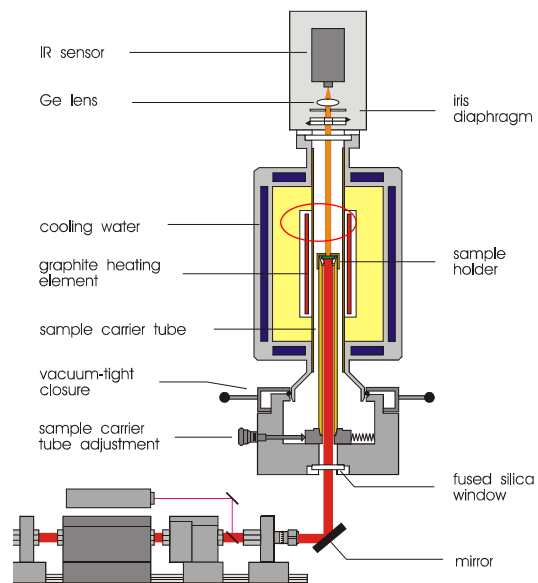
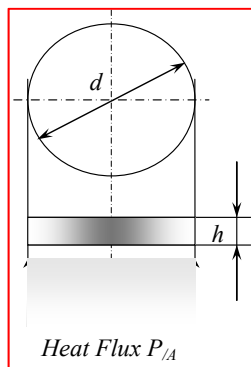


Fig. 10: Laser flash 427 with a typical axial symmetric shape of a specimen for flash experiments

### 4.3.2 Principle of Measurement

As a matter of principle the method operates isotherm and quasi-adiabatic. Different gases can be used. Preferably vacuum conditions ( $p_{min} = 10^{-5}$  mbar) are chosen. In case of low temperature measurements the LFA device is operated under Helium conditions to ensure sufficient thermal link between the sample and

the furnace. Coplanar discoid samples of a height  $h$  as shown in *Fig. 10* and *Fig. 11* (green) are used. If necessary they are sandblasted immediately before the measurement and/or coated with graphite (metallic bright specimen) or gold (transparent specimen). This is in accordance with the relevant standards (Tab. 1) and leads to sufficiently low uncertainties. Details of service conditions are documented in the data sheets of any order (appendix). Based on measurements with reference materials<sup>3</sup> the uncertainty is less than 1% of the measured value.

The measuring process is done in one step and is based on the detection of the time dependent temperature curve at the rare side of the specimen (averted from the laser heated top side of the specimen) after a laser pulse as shown in *Fig. 11*. The data relevant to determine the thermal diffusivity are the maximum temperature increase at the rare side  $T_{max}$  and the time till half of this temperature increase occurs  $t_{1/2}$ . From statistical reasons at a given temperature repeated measurements are done.

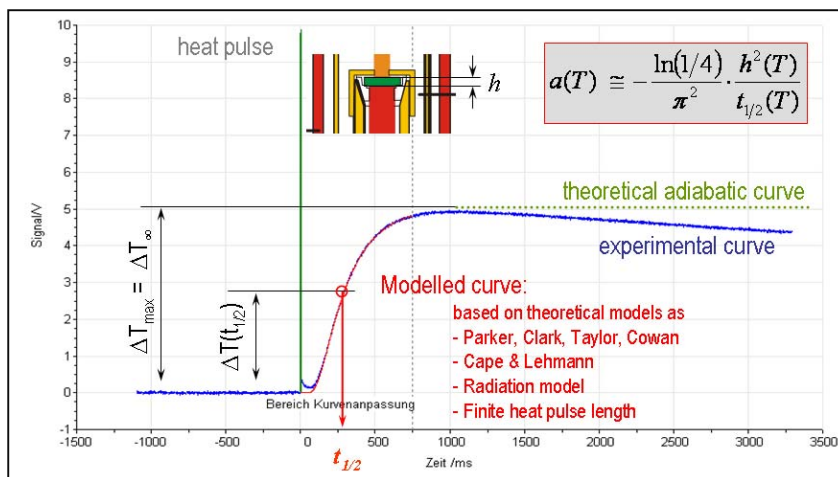


*Fig. 11: Time dependent temperature curve at the rare side of the specimen after a laser pulse*

The solution of the thermal conductivity equation (3.1-4) for a one dimensional problem is given (3.1-5). In case of flash experiments, an infinitely short initial heat impact (initial condition) and adiabatic boundaries are assumed. This means that an ideal thermal insulation of the considered volume is assumed. After the initial heat impact applied by a laser pulse no further heat exchange between the specimen und the thermal environment occurs. Thus, any heat flux vanishes at the surfaces of the considered volume. Mathematically this is formulated with a vanishing temperature gradient at any surface as formulated in equation (4.3-1). In case of a thin and flat body (c.f. *Fig. 10*), influences of the barrel of the specimen are assumed to be negligible. Thus, boundaries must be fulfilled at the bottom and the top surface only. As initial condition at  $t = 0$  an initial heat impact with an infinitesimal short duration at the bottom side of a flat body is required, described by a Dirac delta function  $\delta(t - 0)$  as given in (4.3-2).  $A$  is the surface where the heat impact occurs. These conditions formulate the basic assumptions of Parker's description of a flash technique. The temperature response of the specimen at it's top side is illustrated in *Fig. 11*. It shows both the theoretically calculated temperature characteristic based on the assumption of adiabatic conditions, and the real experimentally detected temperature curve  $T(t)$ . To find a simple and feasible procedure to extract the thermal diffusivity  $a$  from this experimental data a half time  $t_{1/2}$  is defined as the time when half the maximum temperature increase  $0,5 \cdot \Delta T_{\infty} = \Delta T(t_{1/2})$  occurs. Parkers model results to equation (4.3-3).

<sup>3</sup> Typically Steel 4970, Pure Iron, Graphite, Silicon Carbide, Pyroceram

$$\bar{P}_{/A}(\bar{x}, t) \Big|_F = \frac{\partial T(x, t)}{\partial x} \Big|_F = 0 \quad \rightarrow \quad \frac{\partial T(x, t)}{\partial x} \Big|_{x=0} = \frac{\partial T(x, t)}{\partial x} \Big|_{x=h} = 0 \quad (4.3-1)$$

$$\Delta Q(\Delta T_i) = \int_{-\infty}^{\infty} P_{/A} \cdot \delta(t-0) \cdot A \cdot dt \quad (4.3-2)$$

$$a(T) = - \frac{\ln(\frac{1}{4})}{\pi^2} \cdot \frac{h^2(T)}{t_{1/2}} \quad (4.3-3)$$

Since 1961 manifold improvements of Parkers method were done<sup>11 - 16</sup>. Most of them use improved routines to calculate  $a$ , and regard to heat losses at the surfaces of a specimen and the finite length of the laser pulse. Even methods to evaluate temperature responses from thermally transparent materials, multi-layer structures, or multi-dimensional structures are available. These models are scope of delivery in today's flash software. The evaluation techniques implement theoretical descriptions of specific material effects in numerically based routines to fit the measured  $T(t)$  curve. The thermal diffusivity is a parameter in these procedures and can be extracted therefore.

### 4.3.3 Uncertainty Concept:

Application of equation (3.2-7) to equation (4.3-3) only estimates the "Equipment Specific Uncertainty": *ESU* of the flash setup (4.3-4). Notice that Parkers model is used to calculate this expression of the *ESU*! Thus no heat losses of the measured sample and no effects caused by a finite duration of the laser pulse are taken into account. Nevertheless, Parker's equation considers time resolution of the temperature sensor of the LFA, and the accuracy of the thickness detection of the sample as well. Thus, this model describes sufficiently the performance of the measurement setup.

Left side of Fig. 12 shows the diffusivity evaluated from samples of a thickness between 0,1 mm and 1,5 mm up to a maximum detected half time of 20 ms. The right image shows the relative "Equipment Specific Uncertainty": *ESU* correlated to the values of the diffusivity. Uncertainty values are given for a confidential interval of 95%.

$$ESU^2(a) = a^2 \cdot \left[ \frac{4 \cdot u^2(h)}{h^2} + \left( \frac{a \cdot \pi^2}{\ln(1/4) \cdot h^2} \right)^2 \cdot u^2(t_{1/2}) \right] \quad (4.3-4)$$

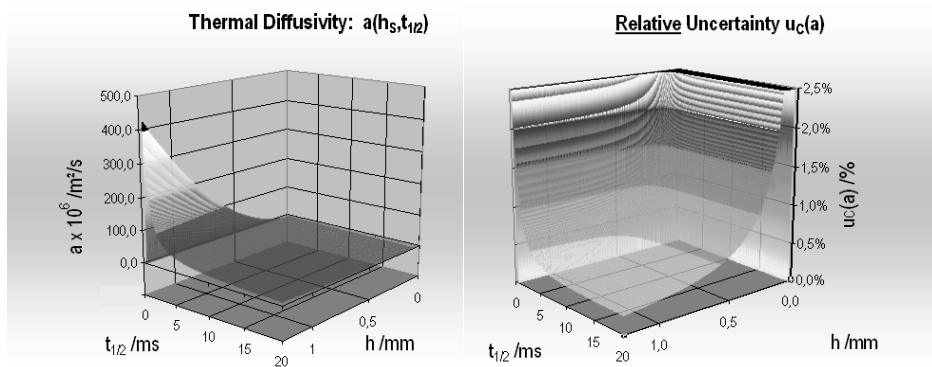


Fig. 12: Diffusivity results (Parker model) and relative uncertainty  $u_c(a)$  as a function of sample thickness and half time  $t_{1/2}$

Combining the evidence from both images enables to state, that an optimum sample thickness can be defined following the principle: the higher the diffusivity of a material is the thicker the sample should be. Following this philosophy the uncertainties of the measured values will be lower than 1% of the measured values.

Equation (4.3-4) strongly depends on the uncertainties of measurement of the thickness  $h$  of the sample and the running time measurement realised in the laser flash setup. This makes clear that the method depends on both coplanar samples and an accuracy of the measurement of the thickness of the sample of a few  $\mu\text{m}$ , and a high resolution of the running time measurement in the flash equipment as well. Modern systems<sup>17</sup> provide a data acquisition rate of about 0,5 MHz. Thus the minimum uncertainty  $u(t_{1/2})$  is 2  $\mu\text{s}$ . The numerical simulation of the measured temperature profile at the top side of the specimen needs about 250 data points between the release of the laser and the half time. Thus a minimum half time of  $t_{1/2}^{(\text{min})} = 0,5 \text{ ms}$  must not be gone below. Thus a minimum sample thickness dependent from the diffusivity of the measured material must not be undergone! Using the LFA performance data as mentioned above, from equation (4.3-3) the estimating expression (4.3-5) can be derived.

$$h_{\text{min}} \cong \sqrt{\frac{\pi^2}{\ln 4} \cdot a \cdot t_{1/2}^{(\text{min})}} \cong 0,06 \cdot \sqrt{a} \quad (4.3-5)$$

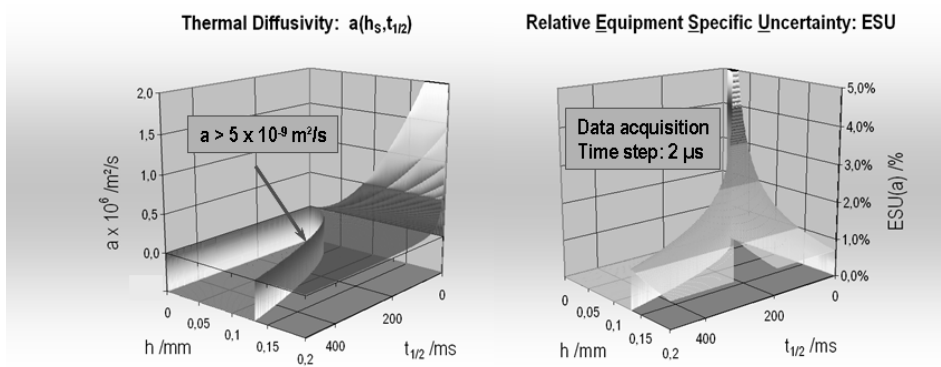


Fig. 13: Limitation of flash method to minimum sample thickness determined by the data acquisition rate of the experimental setup.

Some numerical results thereof are given in Fig. 14. The consequences from equation (4.3-5) are illustrated in Fig. 13. The step in the left curve indicates the interrelationship between the detectable diffusivity and the minimum sample thickness. As a consequence of both thin samples and short half times the increase of the “Equipment Specific Uncertainty”: *ESU*. It is caused by the limitations intrinsically given by the equipment. Nevertheless Fig. 13 shows that even films with a thickness of about 0,02 mm can be measured. Fig. 14 shows that there are no significant restrictions to highly conductive materials as copper, silver or diamond. In case of practical operation some 5000 data points ( $\Sigma_P$ ) will be detected within a material specific observation time typically within a range of  $10^1 \text{ ms}$  and  $10^4 \text{ ms}$  ( $t_M$ ). This defines the uncertainty  $u(t_{1/2})$  attributed to a specific measurement:  $u(t_{1/2}) = t_M / \Sigma_P$ .

Material	$a(T_r) \times 10^6 / \text{m}^2/\text{s}$	$h_{\min} / \text{mm}$
Diamond	1000	1,90
Silver	174	0,79
Copper	117	0,65
POCO AXM 5Q	72	0,51
Pure Iron	22	0,28
Alumina	10,5	0,19
Stainless Steel; AISI 316	3,25	0,11
Pyroceram	1,92	0,08
Glass	0,7	0,05
Filled Polymeres	0,5	0,04
Polycarbonate	0,15	0,02
Paper, PP, ÜTFE	0,1	0,02

Fig. 14: Diffusivity and resulting minimum sample thickness for flash measurements.  
 $t_{1/2}^{(min)} = 0,5 \text{ ms}$  is assumed

To calculate the standard uncertainty of a flash result, additionally to the  $ESU(a)$  the Modell Specific Uncertainty  $MSU(a)$  and the statistical spread of a set of samples  $SDV(a) = SSU(a)$  must be taken into account. Under the consideration of best practice measurements the arithmetic mean of individual measurement results  $a_k$  is the best estimate of the output estimate of  $a$ . As explained in chapter 3.2, zero quantities are added to the mean of input estimates. This still consequences the arithmetic mean to be the best estimate of the measurement result. From postulate, the uncertainties of these zero quantities are attributed to equipment related effects –  $ESU$ , to model related effects –  $MSU$ , and to sample related effects –  $SSU$ : The model is illustrated in Fig. 15.

To estimate  $MSU(a)$  the type B procedure of the GUM is used. Deviations of the half time in dependence from two modelled temperature responses – capturing 5% of the measured temperature data and 95% respectively – are analysed. So far necessary the corresponding slopes of the response curves are taken into account. The uncertainty of this individual diffusivity is measured from the width of the interval  $[a_{95\%}, a_{5\%}]$ . Defining  $[a_{(90)}] := |a_{95\%} - a_{5\%}|$  the GUM teaches:  $u^2(a_i) = [a_{(90)}]^2/3$ . Details of the concept are shown in Fig. 16.

# Applications

... Laser Flash Method

$$Y = f(X_1, X_2, \dots, X_L, \dots, X_N)$$

$$y = f(q_1, q_2, \dots, q_L, \dots, q_N)$$

$$\bar{q} = \frac{1}{n} \cdot \sum_{k=1}^n q_k$$

$$s(q_k) = \sqrt{\frac{1}{n-1} \cdot \sum_{k=1}^n (q_k - \bar{q})^2}$$

$$u(\bar{q}) = \frac{1}{\sqrt{n}} \cdot s(q_k) := u(x_i)$$

$$u_c^2(y) = \sum_{i=1}^N \left( \frac{\partial f}{\partial x_i} \right)^2 \cdot u^2(x_i)$$

$$a(T) = \frac{-\ln(1/4) \cdot h^2}{\pi^2 \cdot t_{1/2}}$$

$$a = \frac{1}{n} \cdot \sum_{k=1}^n a_k + \sum_{j=1}^m C_j; \quad C_j := 0 \forall j$$

$C_S := 0$  ... Correction from Sample Specific Effects

$C_M := 0$  ... Correction from Model Specific Effects

$$u_c^2(a) = \sum_{i=1}^N \left( \frac{\partial f}{\partial x_i} \right)^2 \cdot u^2(x_i) + u^2(C_S) + u^2(C_M)$$

$$u_c^2(a) = ESU^2(a) + SSU^2(a) + MSU^2(a)$$

ESU: Equipment Specific Uncertainty  
 SSU: Sample Specific Uncertainty  
 MSU: Model Specific Uncertainty

$$ESU^2(a) = a^2 \cdot \left[ \frac{4}{h^2} \cdot u^2(h) - \left( \frac{a \cdot \pi^2}{\ln(1/4) \cdot h^2} \right)^2 \cdot u^2(t_{1/2}) \right]$$

$$SSU^2(a) = s^2(a) = \frac{\sum_{k=1}^n (a_k - \bar{a})^2}{n \cdot (n-1)}$$

$MSU^2(a)$  .... from individual  $T(t)$  response

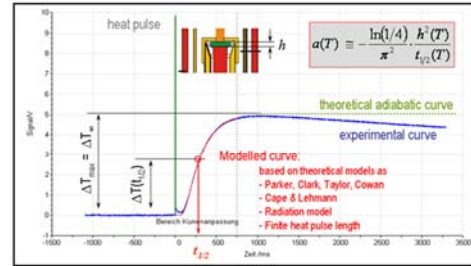


Fig. 15: Concept to formulate uncertainty contributions in Laser Flash measurements

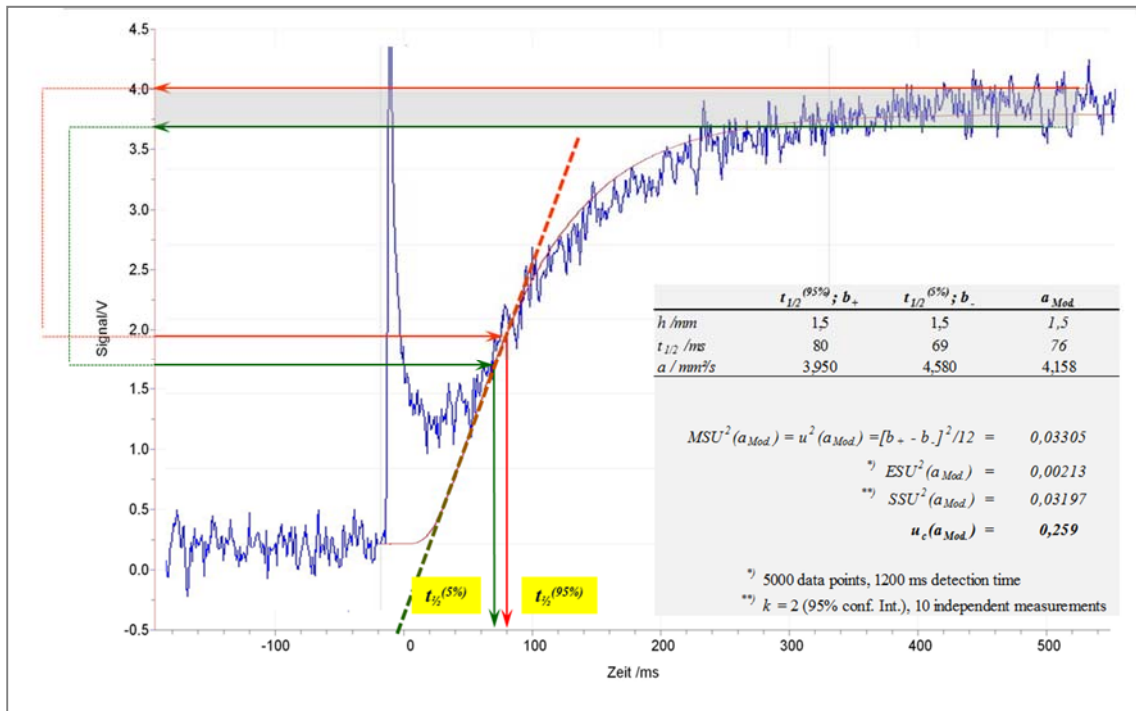


Fig. 16: Basics to estimate  $MSU(a)$  of an individual laser flash experiment

#### 4.3.4 Influence of coatings (transparent samples, ...):

In case of IR-transparent materials, of materials with high IR- reflectance, or in case of thin samples with significant surface roughness, coatings are deposited on both sides of the sample. (For graphite coatings  $a_C \cong 8,5 \cdot 10^{-6} \text{ m}^2/\text{s}$ ). Thus, additionally to the sample thickness  $h_s$  the thickness of the coated layers  $h_c$  must be considered. Notice, that in case of coated samples the measurement procedure identifies an “effective” thermal diffusivity  $\bar{a}$ . From a set of measurements with different numbers of coating layers, the extrapolation to a total coating thickness of  $h_{i,coat.} = 0$  gives a sufficient estimation of the real value of the thermal diffusivity  $a_s$  of the sample itself. The procedure is illustrated in Fig. 17.

The comparison of diffusivity results evaluated from the extrapolation process with diffusivity data from an uncoated thin sample with a significant surface roughness underlines the demand of the method. Correct interpretation of this comparison is, that the factual sample thickness of the uncoated sample (which is relevant for the evaluation of transient thermal transport behaviour of the sample) could not be determined sufficiently – resulting in a severe misinterpretation of the LFA response signal to severely reduced diffusivity data ranging about 50% lower than the real value.

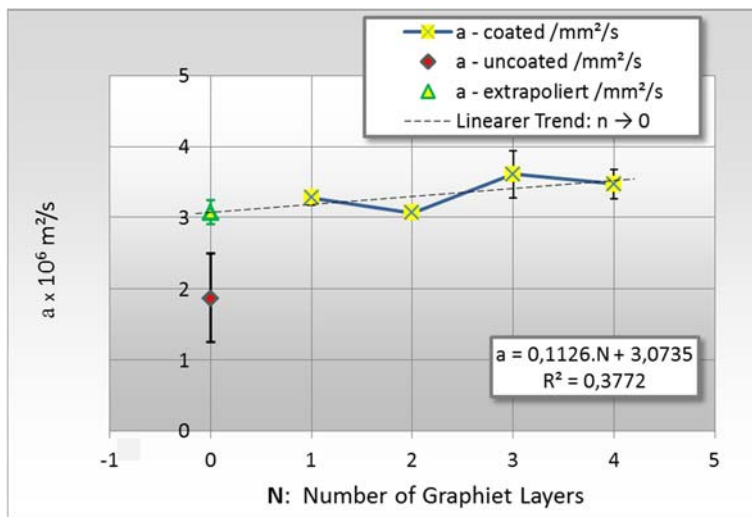


Fig. 17: Extrapolation to a total coating thickness of Zero ( $N = 0$ ) from a set of measurement with different coating thicknesses

#### 4.3.5 Results of Flash Measurements:

For example in a temperature range [-120°C, 1600°C] thermal diffusivity  $a$  (left) and the thermal conductivity  $\lambda$  (right) of a graphite material is shown in Fig. 20. In accordance to (3.1-4) conductivity is calculated from diffusivity, density and specific heat. In a temperature range [-120°C, ~400°C] data from the low-temperature-set up are used. Here values for the  $MSU_{Ia}$  correspond slightly to  $a$ . They scale approximately with 0,5% of the measured diffusivity. Values for the  $ESU_{IcP}$  correspond directly with  $a$  and scale maximum 1% of the measured diffusivity. The combined standard uncertainty of a thermally inert material like graphite can be estimates with approximately 0,5% of the measured value.

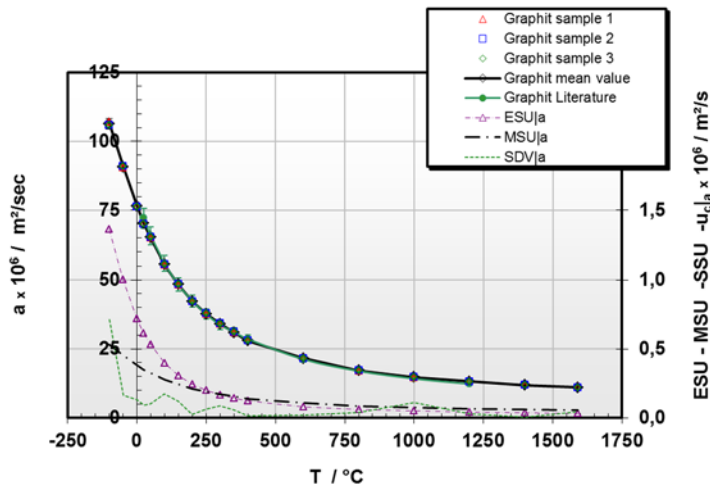


Fig. 18: Thermal diffusivity  $a$ , from a graphite material.

#### 4.3.6 Thermal Conductivity – Examined from Flash Measurements:

The product of measured data of thermal density  $\rho$ , specific heat  $c_p$  and thermal diffusivity  $a$  results to the thermal conductivity. The uncertainty budget relevant for the calculation and resulting data for a graphite material are given in Fig. 19.

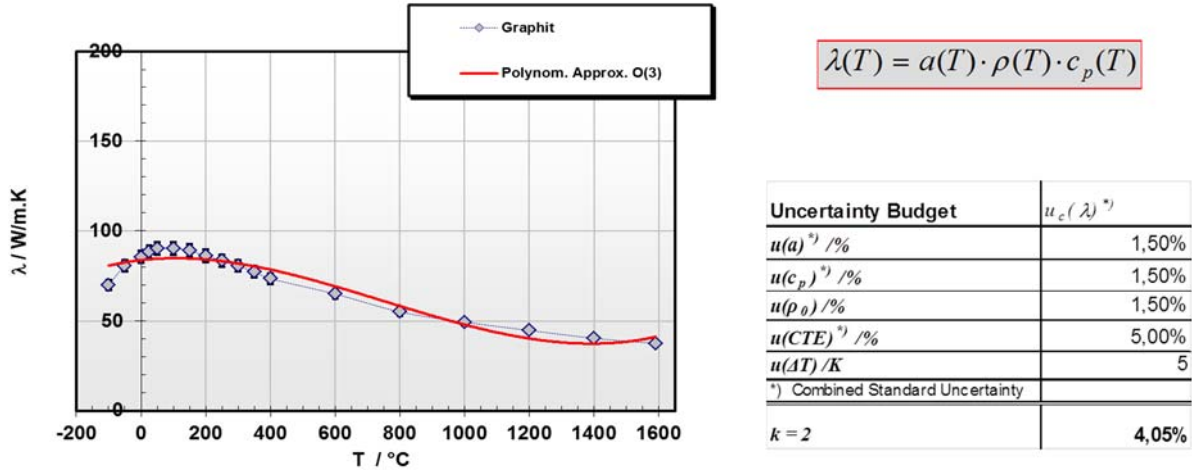


Fig. 19: Uncertainty budget for the thermal conductivity calculated from  $\lambda = a \cdot \rho \cdot c_p$  and calculated data from a graphite material.

A normalized representation of the basic set of thermophysical properties: thermal density  $\rho$ , specific heat  $c_p$ , thermal diffusivity  $a$  and thermal conductivity  $\lambda$  is given in Fig. 20.

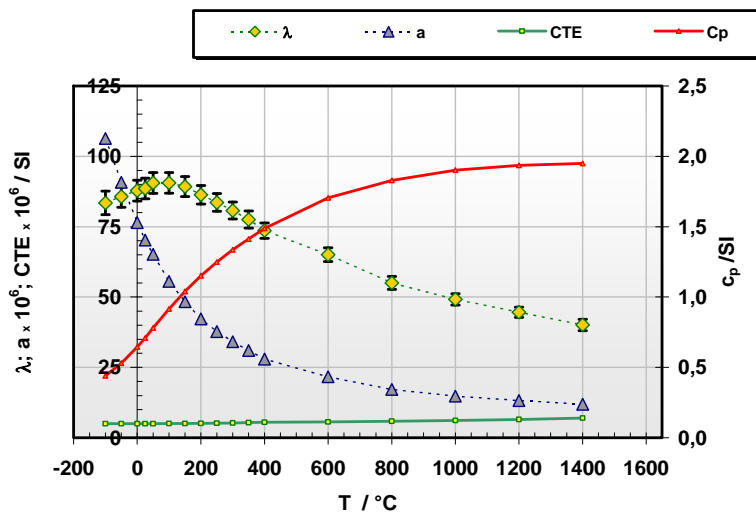


Fig. 20: Overview about the thermophysical data of a graphite material (normalized representation)

## 4.4 Transient Hot Bridge Method THB to measure Thermal Conductivity

### 4.4.1 Measuring Device

The Transient Hot Bridge Method THB measures thermal conductivity. Currently a Linseis THB 100 it is operated under standard atmosphere within a temperature range of  $[-25^{\circ}\text{C}, 250^{\circ}\text{C}]$ . The method is suitable to measure thermal conductivities of solids, weaves, powders or bulk materials and liquids in a range of some  $10^{-3}$  W/m.K up to 5 W/m.K.

### 4.4.2 Principle of Measurement

The method bases on a specific solution of the thermal conductivity equation under transient temperature conditions<sup>18;19;20</sup>. Under ideal experimental conditions two solid blocks with minimum one plan machined surface per each are available. The THB sensor foil is placed between these blocks – ensuring an ideal thermal contact to both of them (Fig. 21). Casually only bulk goods, fabrics or pasts are available. Nevertheless a sufficient thermal contact of both sides of the sensor foil to the specimen can be ensured. Measurements of sufficiently low uncertainty can be achieved.

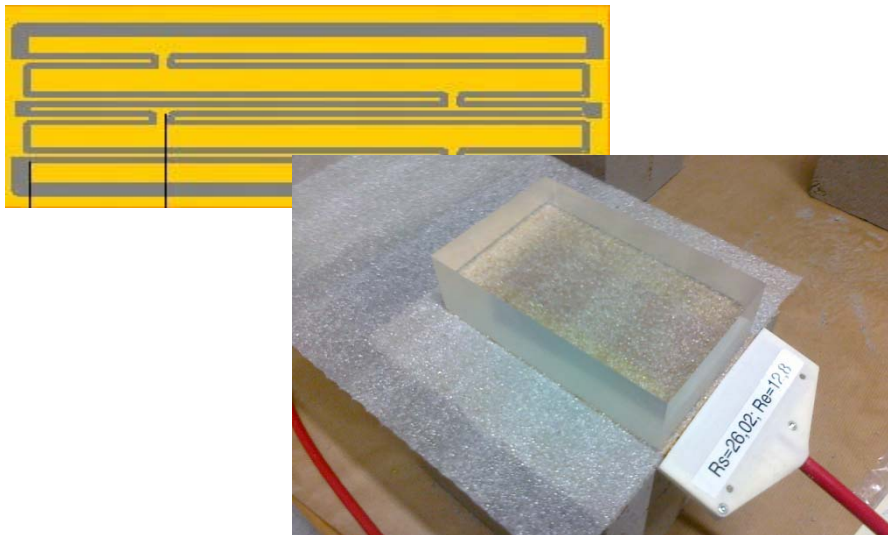


Fig. 21: Scheme of a THB Sensor and measuring approach with two reference BK7 specimen

The sensor operates in two different ways: as a heat source ensuring a constant heat flux and as a detector of the thermal response of the measured material. The method allows to measure thermal conductivity and thermal diffusivity as well. Two different phases of the detected thermal response of the measured sample are used therefor. The initial heating phase allows the examination of the thermal conductivity, the subsequent equilibrium phase from principle allows examination of the thermal diffusivity. A sufficient equilibrium state can only be achieved under ideal experimental conditions. Thus mostly thermal conductivity is measured.

### 4.4.3 Uncertainty Concept:

After calibration of the setup, measurements of a set of reference materials is done. Deviations of the measured data  $q_i$  from literature data  $q_{Lit}$  are used to quantify the *Equipment Specific Uncertainty ESU*. A Type B

evaluation (GUM) is used. Currently, no need to implement a *Model Specific Uncertainty MSU* is identified. *Sample Specific Uncertainty SSU* is calculated from standard deviation of measurement results  $q_s$  of the sample. Equations (3.2-8) and (3.2-9) are used to examine combined standard uncertainty  $u_c(q_i)$ .

#### 4.4.4 Results of THB Measurements:

In Fig. 22 the thermal conductivity of a technical cork material (natural cork pressed with organic binder material) in a temperature range of [-20°C, 100°C] is shown. The influences of the different constituents result in the specific temperature dependence as figured out.

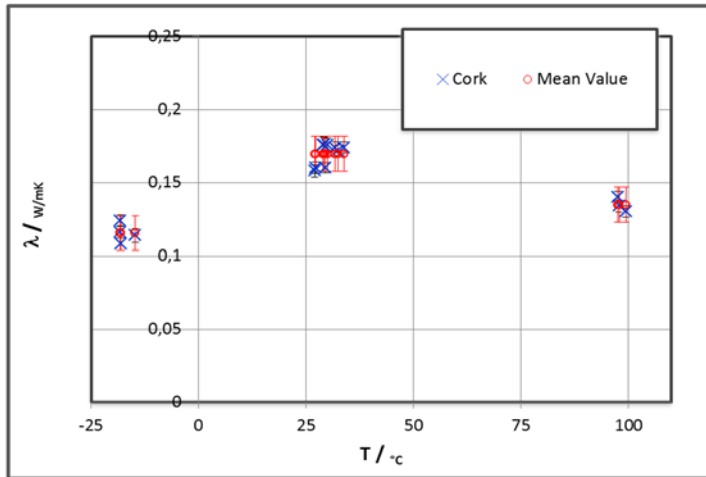


Fig. 22: Thermal conductivity of a cork material measured with the TBH method

## 4.5 Heat Flow Meter Method HFM to measure Thermal Conductivity and Specific Heat

### 4.5.1 Measuring Device

The Heat Flow Meter Method - HFM measures thermal conductivity and specific heat of solids, weaves, bulk goods. A NETZSCH HFM 466 Lambda is in service. The method is suitable to measure thermal conductivity of solids, weaves, powders and bulk materials in a conductivity range of some  $10^{-3}$  W/m.K up to 2 W/m.K. The temperature range of the hot plates is  $[-20^{\circ}\text{C}, 90^{\circ}\text{C}]$ . The temperature difference between both plates is some  $20^{\circ}\text{C}$ . The sample mean temperature is within  $[-10^{\circ}\text{C}, 80^{\circ}\text{C}]$  therefore. Standard operation the HFM is done under ambient pressure conditions and standard atmosphere. In certain cases the test chamber can be flooded with various gases.

### 4.5.2 Principle of Measurement

The method bases on the detection of the time dependent vectorial heat flux  $\vec{P}_{/A}(\vec{x}, t)$  through the sample, and the evaluation of the 1-dimensional representation of equations (3.1-2) and (3.1-3). The medium is assumed to be homogenous. Anisotropic media can be measured, when sample preparation is possible in the relevant directions. Under these requirements, equations (3.1-1) till (3.1-3) simplify to equations (4.5-1) till (4.5-3). One conclusion of this set of equations is (4.5-4).  $A$  represents the cross section of the measured sample,  $h$  its height.

$$Q_V(t) = \rho(T) \cdot V \cdot \left[ \int_0^{T(x,t)} c_p(T) \cdot dT \right] = m \cdot c_p(T) \cdot \Delta T \Big|_{t=0} \quad (4.5-1)$$

$$\vec{P}_{/A} = -\lambda(T) \cdot \nabla T = -\lambda(T) \cdot \frac{\Delta T}{h} = -\frac{\lambda(T)}{h} \cdot \Delta T; \quad \dots R^{(th)} =: \frac{h}{\lambda(T)} \quad (4.5-2)$$

$$Q_V(t) + \int P_{/A}(t) \cdot A \cdot dt = \left\{ \int_{\sum_r S_r^+ + \sum_r S_r^-} dt \right\} \quad (4.5-3)$$

$$Q_V \Big|_T = \frac{\lambda(T) \cdot A}{h} \cdot \int \Delta T(t) \cdot dt \quad (4.5-4)$$



Fig. 23: HFM device NETZSCH HFM 466 Lambda with reference specimen (right, representing typical size of specimen)

To quantify a) heat exchange with the environment and b) parasite heat fluxes off the preferred direction, accurate calibration of the HFM is needed. To guarantee sufficient thermal contact between the heating plates of the device and the sample, from heating plates a defined pressure load of some 2kPa up to 20 kPa is applied. In case of stiff solids, interlayers made up from silicone rubber ensure sufficient thermal contact, and additional thermocouples detect the temperatures from the sample surface (optional instrumentation KIT: c.f. Fig. 24).

Samples thickness must provide a thermal resistance  $R^{(th)}$  ( $\rightarrow$  c.f. equation (4.5-2)) within a range of  $[0,02 \text{ m}^2 \cdot \text{K}/\text{W}; 5 \text{ m}^2 \cdot \text{K}/\text{W}]$ . When the thermal resistance is below  $0,25 \text{ m}^2 \cdot \text{K}/\text{W}$ , the optional instrumentation KIT is applied to improve uncertainty conditions.

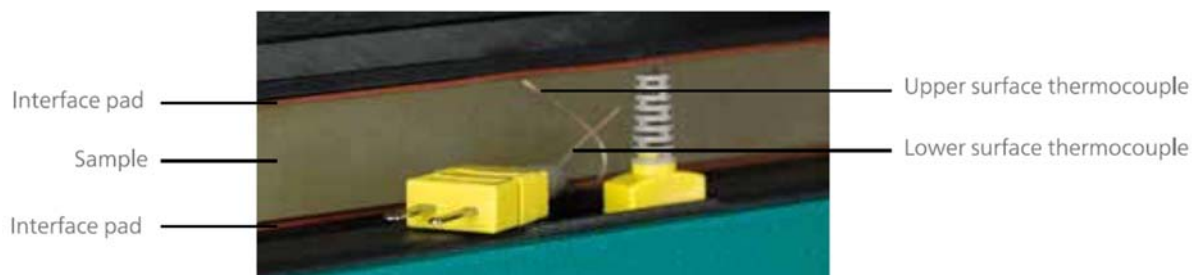
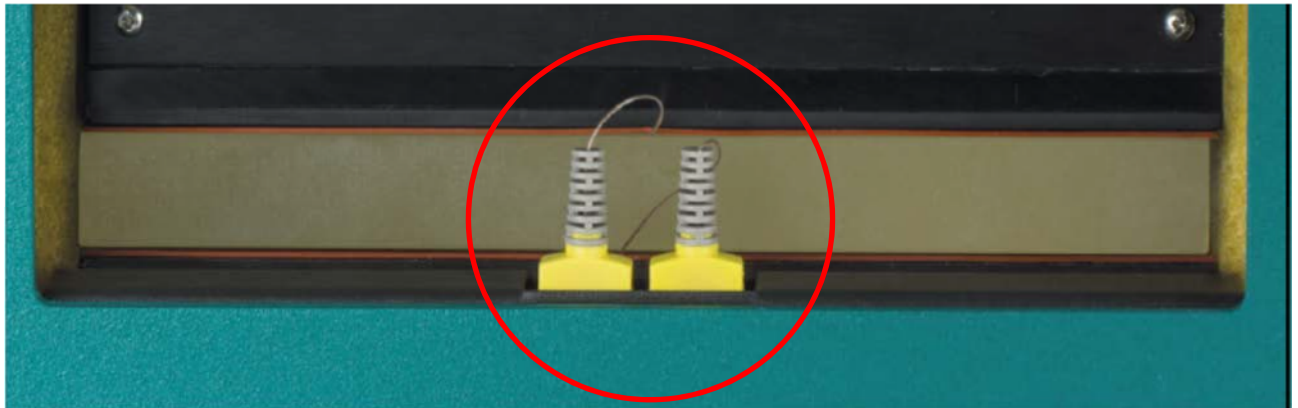


Fig. 24: HFM operation mode with optional instrumentation KIT<sup>21</sup>

### 4.5.3 Uncertainty Concept:

After calibration of the setup, measurements of a set of reference materials is done. Deviations of the measured data  $q_i$  from literature data  $q_{Lit.}$  are used to quantify the Equipment Specific Uncertainty ESU. A Type B evaluation (GUM) is used. Currently, no need to implement a Model Specific Uncertainty MSU is identified. Sample Specific Uncertainty SSU is calculated from standard deviation of measurement results  $q_s$  of the sample. Equations (3.2-8) and (3.2-9) are used to examine combined standard uncertainty  $u_c(q_i)$ .

$$ESU(q_i)^2 = |q_i - q_{Lit.}|^2 \quad (4.5-5)$$

$$MSU(q_i)^2 = 0 \quad (4.5-6)$$

$$u_c(q_i)^2 = ESU(q_i)^2 + SDV(q_i)^2 \quad (4.5-7)$$

### 4.5.4 Results of HFM Measurements:

In Fig. 25 data of thermal conductivity and specific heat of a 4A Zeolith in a temperature range  $[T_R, 75^\circ\text{C}]$  are shown. Specific heat data are compared with results from a DSC measurement. The Zeolite material was exposed to ambient humidity conditions, resulting a 6g/kg humidity load. Thus, DSC data show thermal effects when humidity is released for  $T > 80^\circ\text{C}$ . Within the limits of uncertainties of both methods, good agreement of the data is observed.

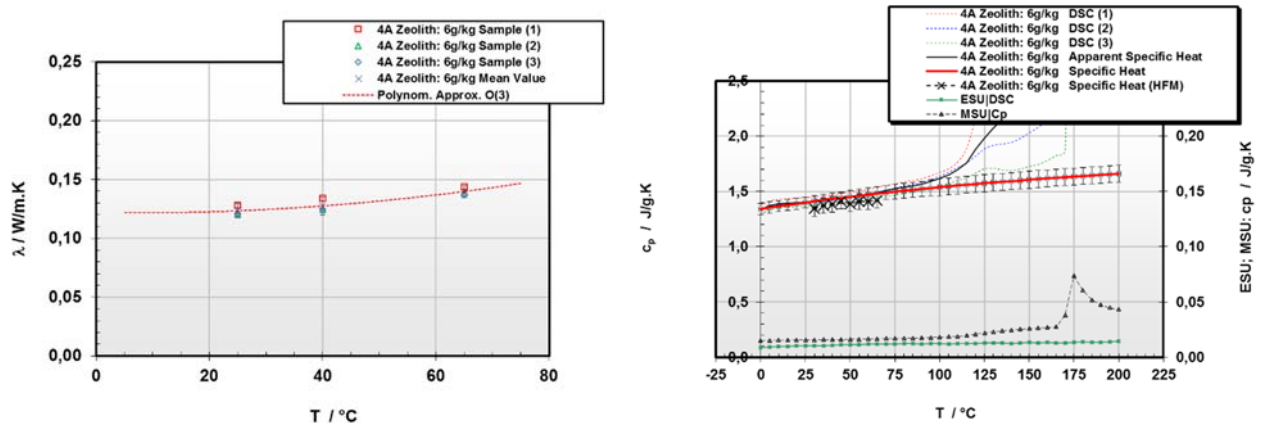


Fig. 25: Thermal Conductivity (left) and comparison of specific heat data (right) measured with DSC and HFM

## 4.6 Simultaneous Thermogravimetry –sDSC; sDTA; QMS; FTIR

### 4.6.1 Measuring Device

The method<sup>22</sup> is used in accordance to the standards listed in Tab.1. Two devices NETZSCH STA 449 F1 Jupiter and a NETZSCH STA 449 F5 Jupiter with an automatized sample changer are in service. Each one is used in a specific temperature range:

- Low temperature STA (NETZSCH STA 449 F1 Jupiter): range of application [-180°C, +1000°C]
- High temperature STA (NETZSCH STA 449 F1 Jupiter, NETZSCH STA 449 F5 Jupiter): range of application [ $T_R$ , +1600°C]



*Fig. 26: Microbalance with simultaneous DTA, DSC, spectroscopy (QMS, FTIR).  
Right: STA-DSC sensor of STA 449 F5 with automatized sample changer*

The top loading microbalance can be operated dynamically and isothermally under different gas conditions as Helium, Argon, Nitrogen, Air, Hydrogen or Forming Gas, etc. – optionally under controlled humidity. Heating rates typically scale between 0,1 K/min and 20 K/min. This is in accordance with the relevant standards (Tab. 1) and leads to sufficiently low uncertainties. The Microbalance shows a digital resolution of 0,025  $\mu\text{g}$  and a maximum load of 5g. The recipient is vacuum tight till  $10^{-4}$  mbar. Details of service conditions are documented in the data sheets of any order (appendix). Based on measurements with reference materials<sup>4</sup> the Equipment Specific Uncertainty is less than 0,01% of the measured value. The Thermogravimetric analysis can be coupled simultaneously with both a Mass Spectroscopy (QMS) Aeolos 403C and a Fourier Transformed Infra-Red Spectroscopy (FTIR) Bruker Tensor 27.

### 4.6.2 Principle of Measurement

Similar to DSC measurements (vgl. Chapter 4.2.2)

### 4.6.3 Uncertainty Concept:

Similar to DSC measurements (vgl. Chapter 4.2.2)

---

<sup>4</sup> Typically Sapphire

#### 4.6.4 Results of TG-sDSC Measurements with simultaneous FTIR & qMS

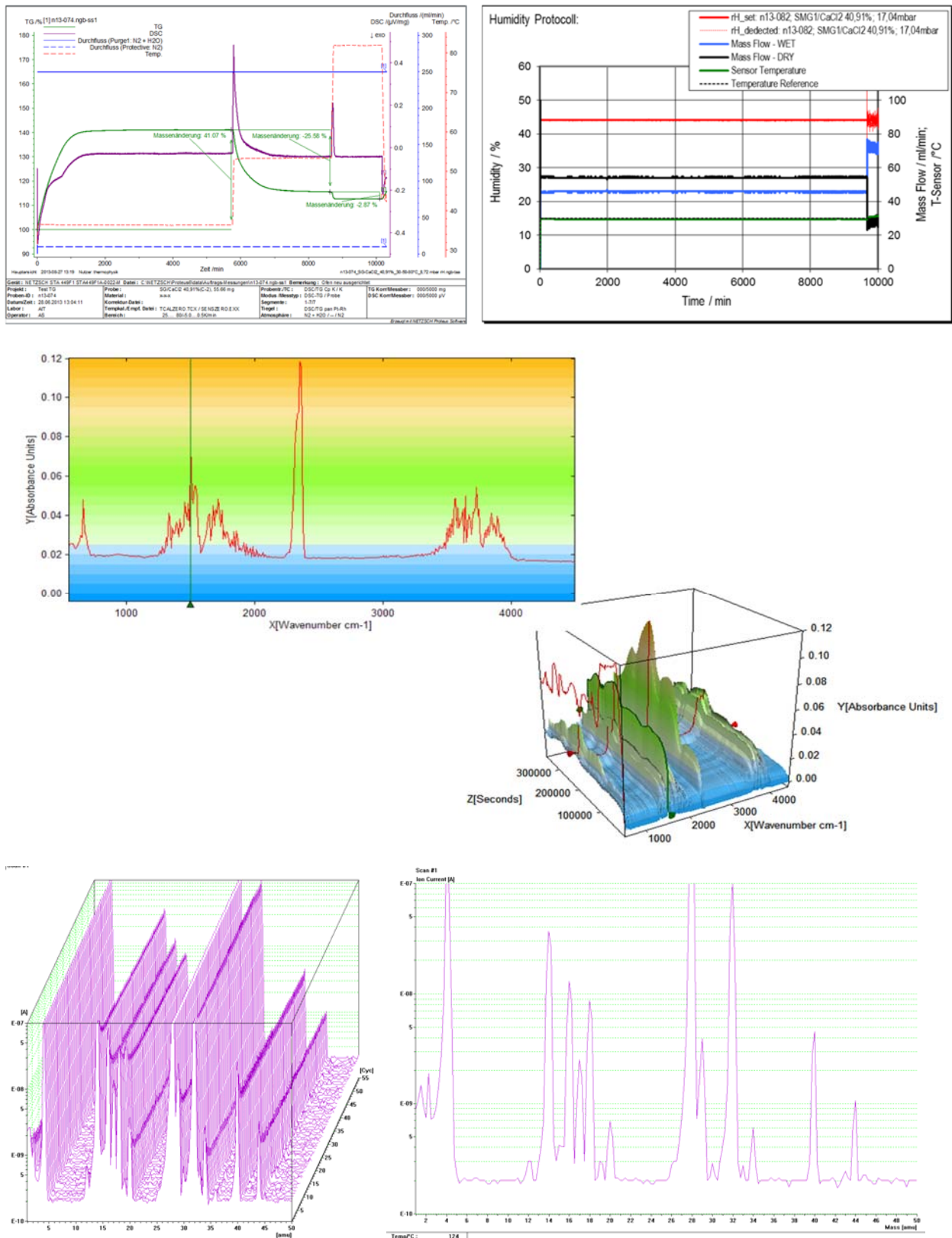


Fig. 27: I) Change of mass of  $\text{CaCl}_2$  (left) under varying humidity conditions (right). Simultaneous DSC plot identifies different hydration steps II, III) Simultaneous FTIR and mass spectroscopy.

## 4.7 Stabinger Viscometry SVM and simultaneous DMA to measure Dynamic & Kinematic Viscosity and Density

### 4.7.1 Measuring Device

The measurement device measures simultaneously dynamic & kinematic viscosity and density of Newtonian liquids. An Anton Paar SVM 3001 Stabinger Viscosimeter is in service. In standard operation the method is operated under standard atmosphere but flushed with 5.0 Nitrogen within a temperature range of [-60°C, 90°C].

### 4.7.2 Principle of Measurement

Analysis of U-tube oscillation is used to determine the density of the measured liquid. The ratio of the rotational frequencies of an outer cylindrical tube, which is filled with the liquid, and a concentric positioned, but inertial stabilized inner cylinder, which is inductively damped, is the primary measurement signal, examined to basic viscosity information. High sophisticated numerical routines are applied to separate hydraulic effects and to quantify viscosity. Accurate calibration of the SVM device is needed.



Fig. 28: Stabinger Viscosimeter SVM 3001

### 4.7.3 Uncertainty Concept:

After calibration of the setup, measurements of a set of reference materials is done. Deviations of the measured data  $q_i$  from literature data  $q_{Lit.}$  are used to quantify the Equipment Specific Uncertainty ESU. A Type B evaluation (GUM) is used. Currently, no need to implement a Model Specific Uncertainty MSU is identified. Sample Specific Uncertainty SSU is calculated from standard deviation of measurement results  $q_S$  of the sample. Equations (3.2-8) and (3.2-9) are used to examine combined standard uncertainty  $u_c(q_i)$ .

$$ESU(q_i)^2 = |q_i - q_{Lit.}|^2 \quad (4.7-5)$$

$$MSU(q_i)^2 = 0 \quad (4.7-6)$$

$$u_c(q_i)^2 = ESU(q_i)^2 + SDV(q_i)^2 \quad (4.7-7)$$

### 4.7.4 Results of SVM Measurements:

In Fig. 29 dynamic & kinematic viscosity and density of a Newtonian liquid is shown. As a consequence of density data approximately like 1, no significant difference between both viscosity data occurs. As expected, temperature dependence of density is linear with  $T$ . Strong dependence of viscosity data of the liquid is observed (logarithmic scale) is observed.

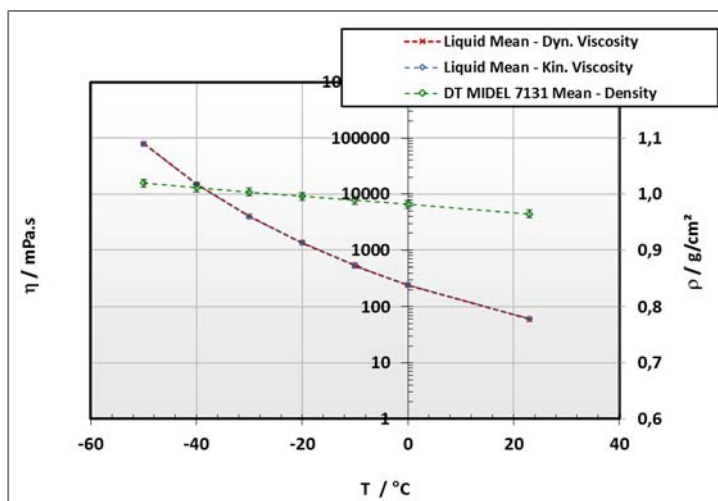


Fig. 29: Dynamic & kinematic viscosity and density of a Newtonian Liquid at low temperatures

It is to be noticed, that even at temperatures significantly above the Pourpoint, local formation of solid clusters can be observed. Cluster formation is statistically and kinetically driven as well. Thus, low temperature data, measured sequentially during cooling down the liquid, might not sufficiently represent the viscosity behaviour at long time exposure of the liquid at low temperatures. Necessity of long-time measurement of viscosity data is indicated from DSC measurements, which show deviations from theoretically expectable temperature profile of the  $c_p$  data. This is driven from enthalpy effects, which are to be drawn back to solidification/melting of phase precipitations from the liquid. Solid precipitations are thermally effected from dissipative effects caused from the kinetic energy input during the measurement (rotation of tube and magnetic cylinder at different rotational frequencies, and shearing effects therefrom). The holistic behaviour, observed during a longer period of time (e.g. several hours) can only be predicted statistically. As an example for variability of observations Fig. 30 shows the direct comparison of four liquids, measured above the Pourpoint for some six hours. The upper left image shows the converging of viscosity with slight statistically deviations. The upper right image shows the analogous tendency of converging of viscosity with slightly decreasing behaviour

– presumably caused from dissipative input of the rotating cylinders. The lower left image shows the significant decrease of viscosity because of dissipative input of the rotating cylinders after a maximum viscosity at the very beginning of the measurement, and converging of viscosity to lower values. The lower right image shows a statistically driven behaviour of the measured liquid, which indicates a more or the less unpredictable behaviour of the matter either as a fluid or a slush, a slurry, or more or the less as a solid.

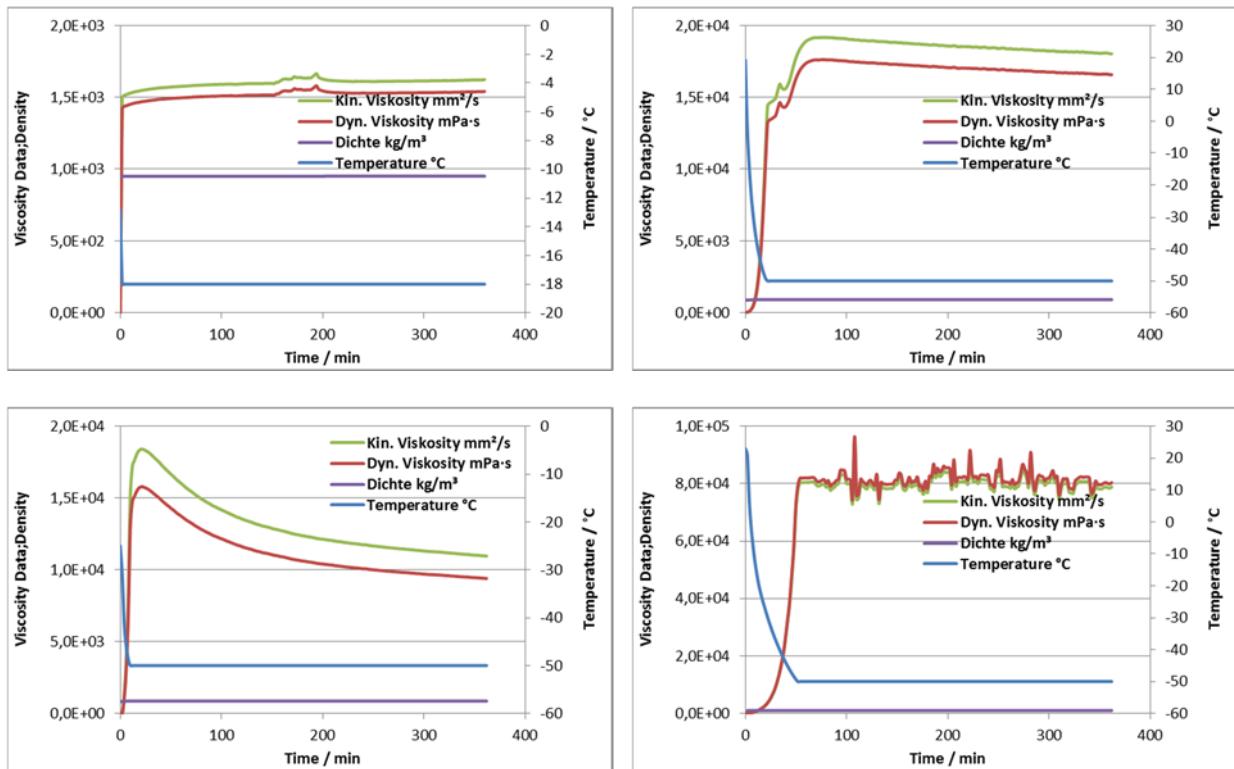


Fig. 30: Direct comparison of viscosity data of four liquids, measured above the Pourpoint for six hours

## 5 Literature

---

- <sup>1</sup> H.S. Carslaw, J.C. Jaeger; Conduction of Heat in Solids; Oxf. Sc. Publ., Reprint 2005, ISBN 0 19 853368 3; (1946)
- <sup>2</sup> [http://phox.at/pdf/Theoretical%20Background%20of%20Flash%20Experiments%20\(05-06-2009\).pdf](http://phox.at/pdf/Theoretical%20Background%20of%20Flash%20Experiments%20(05-06-2009).pdf)
- <sup>3</sup> ENV 13005; Guide to the expression of uncertainty in measurement (1999)
- <sup>4</sup> <http://phox.at/pdf/Messwert%20&%20Messunsicherheit%20-%20Theorie%20und%20Praxisbeispiele.pdf> (2009)
- <sup>5</sup> W.F. Hemminger, H.K. Cammenga; Methoden der Thermischen Analyse, Springer 1989, pp 201-213
- <sup>6</sup> J. Blumm, J. B. Henderson; High Temperatures – High Pressures, 2000, vol. 32, pp 109-113
- <sup>7</sup> <http://phox.at/pdf/Messwert%20&%20Messunsicherheit%20-%20Theorie%20und%20Praxisbeispiele.pdf> (2009)
- <sup>8</sup> W.F. Hemminger, H.K. Cammenga; Methoden der Thermischen Analyse, Springer 1989, pp 100-200
- <sup>9</sup> W. Hohenauer et al; ARC Papers 2004, Thermophysikalische Messverfahren - Kalorimetrie
- <sup>10</sup> W. J. Parker et al; J. Appl. Physics, 1961, vol. 32(9), pp 1679-1684
- <sup>11</sup> F. Rhigini, A. Cezairliyan; Pulse Method of the Thermal Diffusivity Measurement (A Review), High Temp. High Press. Vol.5. 481-501 (1973)
- <sup>12</sup> R.E. Taylor, D.K. Maglic; Pulse Method for Thermal Diffusivity Measurement – in D.K. Maglic, A. Cezairliyan, V.E. Peletsky; Compendium of Thermophysical Property Measurement Methods, Vol.1 Survey of Measurement Techniques; London, Plenum Publishing Corp. (1984)
- <sup>13</sup> L.M. Clark, R.E. Taylor; Radiation Loss in the Flash Method for Thermal Diffusivity; J.Appl.Phys. Vol.46, 714-719 (1975)
- <sup>14</sup> A. Dgiovanni, M. Laurent; Une nouvelle technique d'intification de la diffusivité thermique pour la methode flash; Re- vue Phys. Appl. Vol.21, 229-237 (1986)
- <sup>15</sup> J.A. Cape, G.W. Lehmann; J. Appl. Phys., Vol.34, 1909-1913 (1963)
- <sup>16</sup> J. Blumm, J. Opfermann; Improvement of the mathematical modelling of flash measurements; High Temp. High Press. Vol.34, 515-521 (2002)
- <sup>17</sup> J. Blumm; NETZSCH Gerätebau GmbH, 95100 Selb, Germany; Private Information (2009)
- <sup>18</sup> Hammerschmidt U., Maier V., New Transient Hot-Bridge Sensor to Measure Thermal Conduc- tivity, Thermal Diffusivity, and Volumetric Specific Heat, Int. J. Thermophysics, Vol.27, No.3, pp 840-856, (2006)
- <sup>19</sup> Model R., Stosch R., Hammerschmidt U., Virtual Experiment Design for the Transient Hot-Bridge Sensor, Int. J. Thermophysics, Vol.28, No.5, pp 1447, (2007)
- <sup>20</sup> Hammerschmidt U., Sabuga W., Transient Hot Wire (THW) Method: Uncertainty Assessment, Int. J. Thermophysics, Vol.21, No.6, pp 1255-1278, (2000)
- <sup>21</sup> NETZSCH Gerätebau GmbH, 95100 Selb, Germany; Product Information, HFM\_446\_Lambda\_Series\_de\_web.pdf (26. 03. 2016)
- <sup>22</sup> W.F. Hemminger, H.K. Cammenga; Methoden der Thermischen Analyse, Springer 1989, pp 100-200